

An Amphipathic α -Helix at a Membrane Interface: A Structural Study using a Novel X-ray Diffraction Method

Kalina Hristova¹, William C. Wimley², Vinod K. Mishra³
 G. M. Anantharamiah³, Jere P. Segrest³ and Stephen H. White^{1*}

¹Department of Physiology and Biophysics, University of California at Irvine, Irvine CA 92697-4560, USA

²Department of Biochemistry Tulane University Medical Center, New Orleans LA 70112-2739, USA

³Departments of Medicine and Biochemistry and the Atherosclerosis Research Unit University of Alabama Medical Center, Birmingham AL 35294, USA

The amphipathic α -helix is a recurrent feature of membrane-active proteins, peptides, and toxins. Despite extensive biophysical studies, the structural details of its affinity for membrane interfaces remain rather vague. We report here the first results of an effort to obtain detailed structural information about α -helices in membranes by means of a novel X-ray diffraction method. Specifically, we determined the transbilayer position and orientation of an archetypal class A amphipathic helical peptide in oriented fluid-state dioleoylphosphatidylcholine (DOPC) bilayers. The peptide, Ac-18A-NH₂ (Ac-DWLKAFYDKVAEKLKEAF-NH₂), is a model for class A amphipathic helices of apolipoprotein A-I and other exchangeable lipoproteins. The diffraction method relies upon experimental determinations of absolute scattering-length density profiles along the bilayer normal and the transbilayer distribution of the DOPC double bonds by means of specific bromination, and molecular modeling of the perturbed lipid bilayer (derived using the transbilayer distribution of the double bonds) and the peptide. The diffraction results showed that Ac-18A-NH₂ was located in the bilayer interface and that its transbilayer distribution could be described by a Gaussian function with a 1/e-half-width of 4.5(±0.3) Å located 17.1(±0.3) Å from the bilayer center, close to the glycerol moiety. Molecular modeling suggested that Ac-18A-NH₂ is helical and oriented generally parallel with the bilayer plane. The helicity and orientation were confirmed by oriented circular dichroism measurements. The width of the Gaussian distribution, a measure of the diameter of the helix, indicated that the Ac-18A-NH₂ helix penetrated the hydrocarbon core to about the level of the DOPC double bonds. Bilayer perturbations caused by Ac-18A-NH₂ were surprisingly modest, consisting of a slight decrease in bilayer thickness with a concomitant shift of the double-bond distribution toward the bilayer center, as expected from a small increase in lipid-specific area caused by the peptide.

© 1999 Academic Press

*Corresponding author

Keywords: membrane structure; Ac-18A-NH₂ peptide; phosphatidylcholine bilayer; liquid-crystallography; apolipoprotein A-I

Introduction

The amphipathic α -helix structural motif is frequently encountered in membrane proteins

Abbreviations used: apo A-I, apolipoprotein A-I; DOPC, 1,2-dioleoyl-*sn*-glycero-3-phosphocholine; OBPC, 1-oleoyl-2-(9,10-dibromostearoyl)-*sn*-glycero-3-phosphocholine; HC, hydrocarbon; RH, relative humidity.

E-mail address of the corresponding author: shwhite@uci.edu

(Deisenhofer *et al.*, 1985; Cross & Opella, 1994), plasma lipoproteins (Kanellis *et al.*, 1980; Segrest *et al.*, 1994, 1998), membrane-active toxins (Dempsey, 1990; Tytler *et al.*, 1993; Cramer *et al.*, 1995), and antimicrobial peptides (Maloy & Kari, 1995; Tytler *et al.*, 1995; Tossi *et al.*, 1997). Its structural utility apparently arises from the thermodynamic advantage gained by matching its polar/non-polar surfaces to those of the water/lipid interfaces of micelles and bilayers. Despite the simplicity of this general idea and a large amount of empirical

data (Segrest *et al.*, 1990; Epanand, 1993), quantitative predictions about the interaction of a specific peptide sequence with a particular lipid system are problematic because of the lack of structure-based quantitative principles. These principles are most likely to emerge from coordinated, systematic studies of peptide-bilayer interactions using thermodynamic and direct structural methods (Jacobs & White, 1989; White & Wimley, 1994, 1998; Wimley & White, 1996). Direct structural information about the interactions of peptides with membranes, such as their positions within the thickness of the membrane and the response of the membrane to their presence, is vital for describing the interactions at the molecular level. We report here the first results of an effort to obtain such information using a novel X-ray diffraction method, referred to as absolute-scale refinement, that is derived from so-called liquid crystallography (Wiener & White, 1991c, 1992b; Hristova & White, 1998). Specifically, we have determined the structure of a peptide-bilayer system at low hydration comprised of oriented multilamellar arrays of DOPC bilayers containing the class A amphipathic helical peptide Ac-18A-NH₂ (Ac-DWLKAFYDKVAEKLKEAF-NH₂). We show how absolute-scale refinement can be used to obtain quantitative information about the position of the helix axis relative to the bilayer center and lipid structural groups, the depth of penetration of the helix surface into the bilayer hydrocarbon core, and the perturbations of the bilayer structure caused by the peptide. The ability to obtain such information is essential for testing theories and algorithms that have been developed for predicting the orientation and the penetration depth of amphipathic helices in lipid bilayers based upon amino acid sequence (Segrest *et al.*, 1974; Brasseur *et al.*, 1988; Brasseur, 1991; Jones *et al.*, 1992; Palgunachari *et al.*, 1996).

Ac-18A-NH₂ is an 18-residue peptide that mimics α -helical segments of exchangeable human apolipoproteins, especially apolipoprotein A-I (Anantharamaiah *et al.*, 1985; Venkatachalapathi *et al.*, 1993; Mishra *et al.*, 1994), which is the main component of high-density lipoproteins (HDLs) that consists of 243 amino acid residues with ten putative tandem 22-mer amphipathic α -helical repeats. A crystal structure of apo $\Delta(1-43)$ A-I determined at 4 Å resolution (Borhani *et al.*, 1997) in the absence of lipid reveals a pseudo-continuous amphipathic α -helix that is punctuated by proline residues. The majority of the apo A-I repeats are class A amphipathic helices (Segrest *et al.*, 1992, 1994; Spuhler *et al.*, 1994), which have positively charged amino acid residues at the polar-non-polar interface and negatively charged amino acids at the center of the polar face (Segrest *et al.*, 1998). Previous studies have shown that the helicity of Ac-18A-NH₂ increases from 55% in water to 72% when bound to lipid vesicles (Mishra *et al.*, 1994). Because it can form an amphipathic helix with well-defined hydrophilic and hydrophobic surfaces, Ac-18A-NH₂ has been assumed to bind to

bilayer interfaces with its helix axis parallel with the bilayer surface.

Diffraction-based structural studies of fluid (L _{α} -phase) lipid bilayer systems, especially those containing peptides and proteins, present special challenges. Atomic-level three-dimensional structural models cannot be obtained because of the extreme thermal motion of the lipids and water and consequent lack of crystalline order in the plane of the membrane. However, because fluid bilayers can be formed into oriented multilamellar arrays with high spatial coherence, diffraction can be used to obtain one-dimensional "structures" that represent the projection of the thermally disordered contents of the unit cell on to an axis normal to the bilayer surface (Franks & Levine, 1981). These low-resolution structures, called bilayer profiles, generally provide only rudimentary structural information. However, their effective resolution can be improved through determination of the positions within the profiles of particular lipid atomic groups or bound peptides by means of specific deuteration and neutron diffraction (Büldt *et al.*, 1978; Jacobs & White, 1989; Bradshaw *et al.*, 1994) or specific bromination and X-ray diffraction (Franks *et al.*, 1978; Wiener & White, 1991c; Hristova & White, 1998).

Wiener & White (1991a,b) extended this approach by developing liquid crystallography for the determination of complete one-dimensional structures of fluid (liquid-crystalline) bilayers (reviewed by White & Wiener, 1995, 1996). This method, which combines X-ray and neutron diffraction data using a crystallographic refinement approach, yields the positions and transbilayer spatial distributions of the water and the principal lipid structural groups (carbonyl, phosphate, choline, etc.), referred to as component groups (Petrache *et al.*, 1997) or quasimolecular fragments (King & White, 1986). As for the profiles, these distributions represent the time-averaged projections of the three-dimensional motions of the component groups onto the bilayer normal. The "structure" of the bilayer consists of the complete collection of the component-group distributions. Because of the central-limit theorem (Barlow, 1989), the experimentally determined distributions are invariably Gaussian (Wiener *et al.*, 1991; Wiener & White, 1991c). If a peptide is incorporated into fluid bilayers, the structure of the bilayer-peptide complex is given by the superposition of the transbilayer distribution of the peptide along the bilayer normal and the set of component-group projections. To obtain such a structure using the method described here, the peptide of interest must be introduced into a fluid bilayer whose peptide-free structure is already known. The only fluid bilayer whose structure has been completely solved by liquid-crystallography is DOPC at 66% RH (5.4 water molecules/lipid molecule: Wiener & White, 1992b) and we thus used that system in the present study. Although this may seem to be quite limiting, recent work directed toward obtaining

structures at higher water contents suggests that increased water content does not drastically alter the bilayer structure (Hristova & White, 1998).

The enabling feature of liquid crystallography is the determination of bilayer profiles on an absolute scattering-length density scale. Most X-ray studies report bilayer profiles on a relative scale. As we demonstrate here, little can be learned about the disposition of peptides in membranes using relative-scale structures. An absolute scale is required, the simplest being the so-called relative-absolute scale (Jacobs & White, 1989; Wiener & White, 1991c; Hristova & White, 1998) that normalizes scattering density relative to a single lipid of the bilayer. This per-lipid scale is convenient because it does not require knowledge of the area per lipid in the bilayer. Neutron-determined profiles can be placed on the per-lipid scale using specific deuteration and difference-structure methods (Wiener *et al.*, 1991; Wiener & White, 1992a) if the composition of the unit cell is known. A similar approach can be used for placing X-ray profiles on an absolute scale by using specific bromination (Franks *et al.*, 1978; Wiener & White, 1991c). We showed recently that X-ray diffraction measurements of the transbilayer distribution of the double bonds of phospholipid acyl chains provide information about the structure of the hydrocarbon core that is remarkably sensitive to changes in bilayer structure (Hristova & White, 1998). These absolute-scale measurements utilized an isomorphous variant of DOPC with double bonds specifically labeled with bromine (Br) in the *sn*2 chain to produce 1-oleoyl-2-(9,10-dibromosteroyl)-*sn*-glycero-3-phosphocholine (OBPC; Wiener & White, 1991c).

In the present study, we were able to infer peptide-induced changes in DOPC bilayer structure by measuring the accompanying changes in the Br-labeled double-bond distributions. These changes provided a basis for the accurate determination of the transbilayer distribution of the peptide and for the construction of molecular models for Ac-18A-NH₂ in the bilayer. Models constructed by means of molecular dynamics simulations placed limits on the range of peptide conformations and orientations that could be reasonably expected to occur in the membrane.

Results

Because the transbilayer distribution of lipid component groups of fluid bilayers determined by liquid crystallography are invariably Gaussian (see above), we expected the transbilayer distribution of Ac-18A-NH₂ to be Gaussian as well. That being the case, the first goal of the absolute-scale refinement procedure was to determine the position Z_p and $1/e$ -halfwidth A_p of the peptide's Gaussian envelope. The second goal was to determine through model building the most likely conformation, transbilayer position, and orientation of the peptide consistent with this envelope. The

absolute-scale refinement procedure we adopted to achieve these goals involved four steps. (1) Determination of the X-ray scattering-density profiles of the DOPC bilayer with and without peptide on the per-lipid absolute scale by means of specific bromination of double-bonds. (2) Construction of peptide-perturbed bilayer model structures, based upon the changes in the double-bond distribution and/or Bragg spacing. (3) Determination of the Gaussian distribution that best describes the transbilayer distribution of the peptide. (4) Determination by model building of the range of peptide conformations, positions, and orientations that satisfied this Gaussian distribution.

The last, model-building step was implemented by generating a library of peptide structures using molecular dynamics simulations whose positions and orientations of in the bilayer were optimized by refinement of the calculated structure factors of the bilayer/peptide complex against the observed structure factors. The primary refinement variables used were the position and tilt of the peptide axis and the average crystallographic Debye temperature factor (B) of the peptide's atoms. The B -factor is a measure of the amplitude of the thermal fluctuations of an atom around its mean position (Warren, 1969). By average B , we mean that a single B -factor was applied to all atoms. We assumed that the transbilayer Gaussian envelope of the whole peptide could be obtained by summing the Gaussian scattering-length densities of the individual atoms and that the most likely atomic B -factors would be those that were close to the B -factors of lipid component groups. The latter assumption is reasonable, because the conformational flexibility of the peptide must surely reflect the thermal motion of its surroundings, i.e. the fluid bilayer. This assumption provided the basis for choosing the most likely peptide conformations from the library of peptide structures.

Step 1: X-ray scattering-density profiles of bilayers containing Ac-18A-NH₂

We determined the lamellar structure factors of oriented DOPC/OBPC multilayers containing 5 mol% of Ac-18A-NH₂ (molar ratio 19:1) equilibrated at 66% RH at mol% values of OBPC ranging from 0 to 100 (Table 1). The Bragg spacing (d) of 46.5(±0.5) Å was independent of the mol% OBPC and significantly smaller than the value of 49.1(±0.3) Å observed for peptide-free DOPC bilayers (Wiener & White, 1991c; Hristova & White, 1998). The hydration of the peptide-containing bilayers was determined to be 5.7(±0.2) water molecules/lipid molecule compared to 5.4(±0.1) for peptide-free bilayers (White *et al.*, 1987). These changes in Bragg spacing and hydration indicate that the peptide perturbed the structure of the lipid bilayer. Generally, increases in lipid hydration are accompanied by increases in the area per lipid molecule and an accompanying decrease in hydrocarbon core thickness. The peptide-induced shift of

Table 1. Observed and calculated relative-absolute (i.e. per lipid) structure factor amplitudes for oriented DOPC multilayers at 66% RH without and with 5 mol% Ac-18A-NH₂ (18A)

l^a	DOPC ^b (observed)	DOPC + 18A ^c (observed)	DOPC + 18A ^d (calculated) model bilayer A	DOPC + 18A ^d (calculated) model bilayer B
1	-43.95 ± 0.88	-66.61 ± 4.12	-63.17	-66.88
2	-0.52 ± 0.74	-1.59 ± 0.37	-0.11	-1.44
3	5.15 ± 0.80	17.27 ± 1.25	17.17	17.69
4	-11.97 ± 1.29	-19.32 ± 1.39	-20.05	-18.85
5	3.38 ± 0.32	3.6 ± 0.8 ^e	5.94	4.92
6	-2.47 ± 0.88	n.o. ^f	(-1.61)	(-1.41)
7	2.03 ± 0.65	n.o.	(0.82)	(0.080)
8	-2.24 ± 0.49	n.o.	(-1.02)	(-1.20)

See Wiener & White (1991c) and Hristova & White (1998) for a discussion of the relative-absolute (per lipid) scaling.

^a Diffraction order.

^b Data taken from Wiener & White (1991c).

^c Experimental structure factors ± standard deviation.

^d Calculated structure factors. Values in parentheses are not observable (see the text).

^e Not observed for all OBPC concentrations. As a result, the experimental uncertainty is computed based only on 0 mol% OBPC data.

^f Not observable.

the double bonds toward the bilayer center, described below, is consistent with precisely those sorts of structural perturbations.

Whereas eight lamellar diffraction orders can be observed for peptide-free bilayers (Wiener & White, 1991c; Hristova & White, 1998), only four or five orders of diffraction, depending upon OBPC content, were observed in the presence of Ac-18A-NH₂ because it causes a "smoothing" of the bilayer profile (see below). Four orders of diffraction data are sufficient, however, for determining the fully resolved transmembrane distribution of the double-bond bromine labels and for placing the structure factors of the peptide/bilayer complex on the per-lipid scattering-length density scale, as discussed previously (Hristova & White, 1998). Figure 1 shows that the structure factors depend linearly on mol% OBPC. This observation and the OBPC-independent Bragg spacing of 46.5 Å confirmed that OBPC was isomorphous with DOPC in these experiments.

The per-lipid scattering-density profiles for DOPC/OBPC bilayers with 5 mol% Ac-18A-NH₂ containing 0, 10, 25, 50, 75, or 100 mol% OBPC are shown in Figure 2(a). Figure 2(b) shows the transbilayer distribution of the bromine labels (10, 25, 50, 75 and 100 mol% OBPC) determined from Gaussian fits in reciprocal space to the difference structure factors relative to 0 mol% OBPC. It is these distributions, representing the thermal envelope of the double-bond distribution convoluted with the stationary hard-sphere distribution of the Br atoms (Wiener *et al.*, 1991; Wiener & White, 1991c), that allow the membrane profiles to be placed on the absolute per-lipid scale (see Materials and Methods). The utility of absolute scaling is demonstrated in Figure 3. The relative-scale profiles of bilayers with and without peptide (Figure 3(a)) shows that little information about peptide disposition other than its effect on bilayer thickness can be obtained by comparing the profiles. When

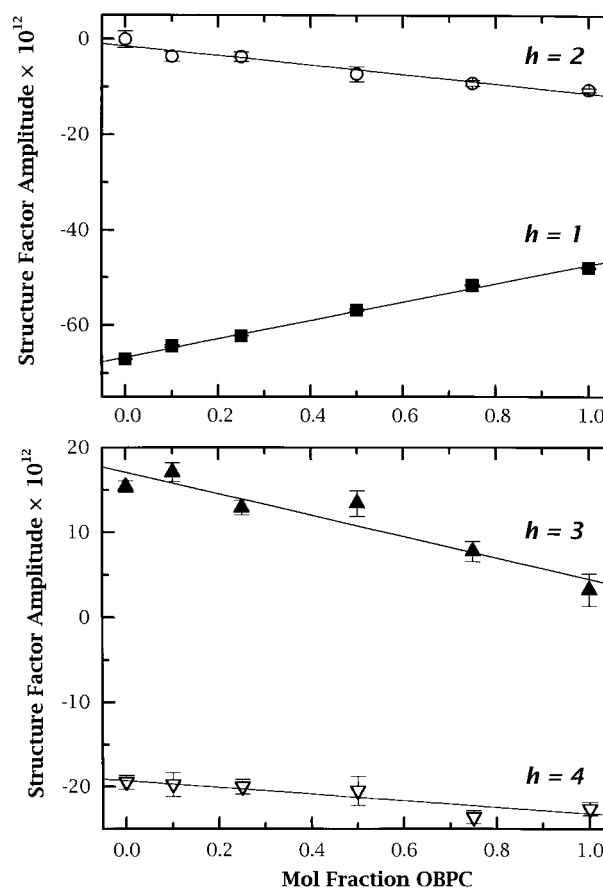


Figure 1. Observed structure factors of OBPC/DOPC bilayers at 66% RH containing 5 mol% Ac-18A-NH₂ as a function of the mol fraction of OBPC. The structure factor amplitudes $F^*(h)$ have been scaled to be on the relative-absolute (per-lipid) scale. The error bars were obtained from the uncertainties in the integrated intensities of the diffraction peaks as described in Materials and Methods. The continuous lines are derived from the self-consistent linear fit to all the data by means of equation (3). For a given OBPC mol fraction, a point on the line represents the best estimate of a per-lipid structure factors, $\tilde{F}^*(h)$.

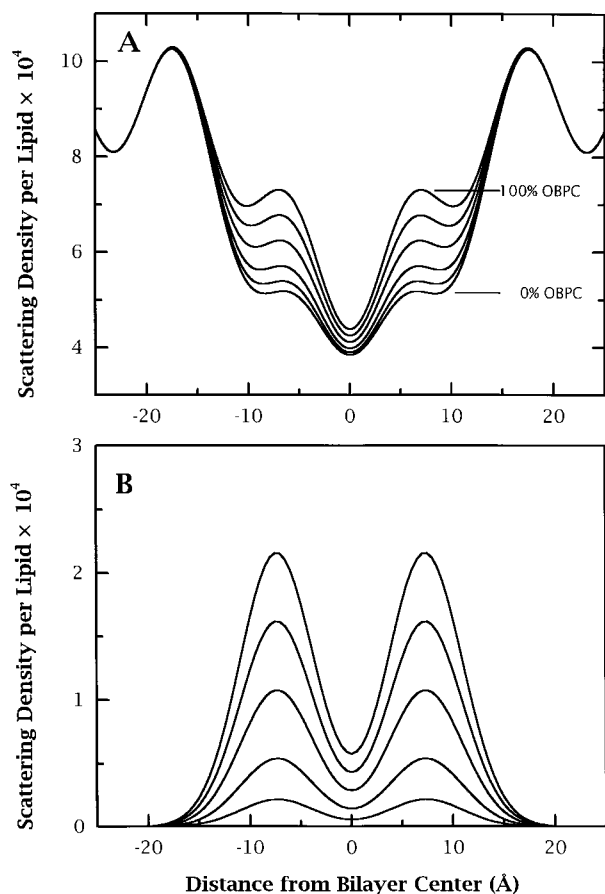


Figure 2. Scattering density profiles of OBPC/DOPC bilayers at 66% RH containing 5 mol% Ac-18A-NH₂ and difference scattering density profiles showing the transbilayer distribution of the bromine labels on the *sn*-2 chain double bond of OBPC. The Fourier reconstructions are generated from the structure factors $\tilde{F}^*(h)$ of Figure 1. (a) Profiles are shown for 0, 10, 25, 50, 75, and 100 mol% OBPC. (b) The difference profiles, indicating the positions of the Br labels on the double bonds, are the Gaussian distributions obtained from fits to the difference-structure factors obtained relative to the 0 mol% OBPC structure factors. The peaks represent 10, 25, 50, 75 and 100 mol% OBPC. The two peaks, located about 7 Å from the bilayer center, increase in amplitude with increasing mol fractions of OBPC.

absolute-scale profiles are compared (Figure 3(b)), however, the approximate location of the peptide is immediately apparent.

The real-space difference of the two profiles in Figure 3(b) (violet dot-dash curve) reveals that the transbilayer distribution of Ac-18A-NH₂ is approximately Gaussian with peaks located at ± 16.6 Å relative to the bilayer center, indicating that the peptide was located in the interface region of the bilayer. Without any further analysis, this difference profile represents a good estimate of the position and width (~ 10 Å) of the peptide distribution. However, real-space difference profiles can be misleading because of differ-

ences in Bragg spacing and unit cell composition. A more accurate description of the peptide distribution requires that the changes in Bragg spacing, unit-cell composition, and bilayer structure be accounted for. That is the purpose of the subsequent stages of the absolute-scale refinement procedure. However, the peptide distribution determined by absolute-scale refinement (below) should not differ from 16.6 Å by more

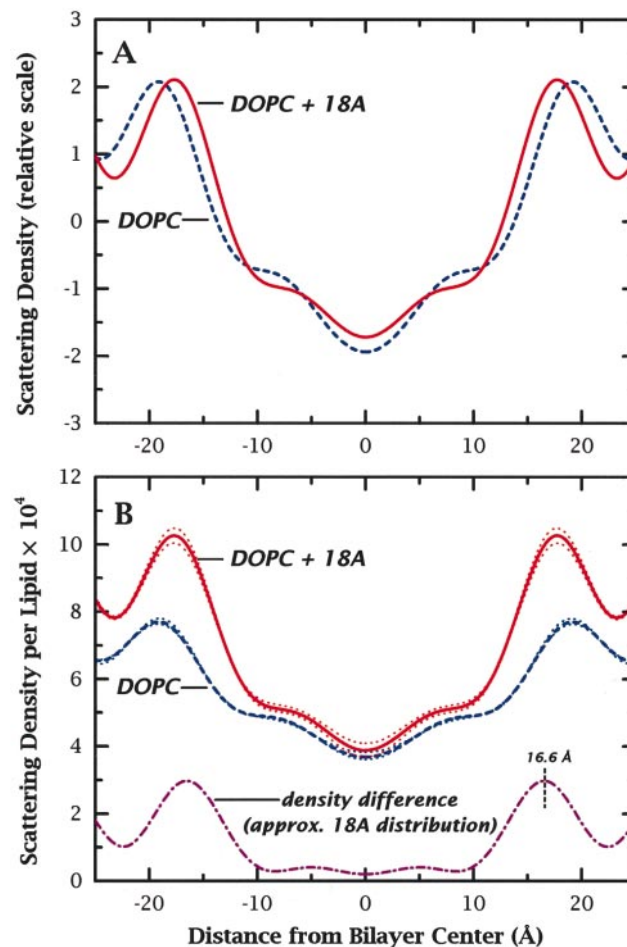


Figure 3. Scattering density profiles of DOPC bilayers with and without 5 mol% Ac-18A-NH₂. (a) Profiles on a relative scattering density scale show fluctuations of arbitrary amplitude around a mean value of 0. A visual comparison of these two profiles provides no information about the location of Ac-18A-NH₂ (18A) in the DOPC bilayer. In order to place profiles such as these on an absolute scale, the mean value of scattering density of the unit cell is added to the profiles and the fluctuations around the mean are calibrated by means of difference structures such as those in Figure 2. (b) The profiles of (a) placed on the per-lipid absolute scale. A visual comparison of the DOPC + 18A profile with the DOPC profile immediately reveals that Ac-18A-NH₂ is located in the headgroup region of the DOPC bilayer. Subtraction of the DOPC profile (broken blue curve) from the DOPC + 18A profile (continuous red curve) shows the approximate distribution of Ac-18A-NH₂ (violet dot-dash curve). The peaks are approximately Gaussian in shape. The dotted lines show the total experimental uncertainties of the profiles.

than about Δd ($1.3(\pm 0.6)$ Å). This allows a rough validation of the subsequent refinement procedure.

Step 2: peptide-perturbed bilayer structure

The perturbation of the bilayer by Ac-18A-NH₂ is revealed directly by the changes in the Br-labeled double-bond distribution, which are quite sensitive to changes in the structure and physical state of the hydrocarbon core of fluid DOPC bilayers (Hristova & White, 1998). Ac-18A-NH₂ caused the double bond to shift towards the bilayer center from $Z_{\text{Br}} = 7.97(\pm 0.27)$ Å to $7.32(\pm 0.12)$ Å ($\Delta Z_{\text{Br}} = 0.65(\pm 0.30)$ Å) without a significant change in its 1/e-halfwidth A_{Br} (Figure 4(a) and Table 2), indicating that the effect of the peptide on bilayer structure was modest. This small, but significant, change in Z_{Br} , consistent with a slight increase in the area per lipid in the bilayer, permitted the change in bilayer structure to be modeled using simple perturbation approaches. Such small changes in Z_{Br} and A_{Br} seem to be peculiar to amphipathic helices at bilayer interfaces. Much larger changes in these parameters have been observed for small unstructured peptides and for transmembrane α -helices (unpublished results).

The determination of models for the perturbed bilayer began with the known structural model of pure DOPC bilayers determined by joint refinement of X-ray and neutron diffraction data (Wiener & White, 1992b). As summarized in Table 3, the neat DOPC fluid bilayer can be represented by ten Gaussian distributions that account completely for the contents of the unit cell. Because the peptide had virtually no effect on A_{Br} and only a small effect on Z_{Br} (Table 2), we constructed two models by keeping the widths of the Gaussians fixed at their peptide-free values and scaling their positions according to the changes in Z_{Br} and/or Bragg spacing (see Materials and Methods). In bilayer model A, the methyl, methylene, and double-bond Gaussian positions of the Wiener & White (1992b) model (Table 3) were scaled by $Z_{\text{Br}}^{\text{DOPC} + 18\text{A}}/Z_{\text{Br}}^{\text{DOPC}}$, while the remaining (interfacial) Gaussian positions (Z_j) were assumed to shift relative to $Z_{\text{Br}}^{\text{DOPC} + 18\text{A}}$ through a scale factor of $([d_{\text{DOPC} + 18\text{A}} - 2Z_{\text{Br}}^{\text{DOPC} + 18\text{A}}]/[d_{\text{DOPC}} - 2Z_{\text{Br}}^{\text{DOPC}}])$. In bilayer model B, all the Gaussian positions of the Wiener & White (1992b) structure were simply scaled by $d_{\text{DOPC} + 18\text{A}}/d_{\text{DOPC}}$. The positions of the Gaussians for the two model bilayers are given in Table 3. The error limits on the positions are determined by the uncertainties in $\Delta Z_{\text{Br}}(\pm 0.30)$ Å and $\Delta d/2(\pm 0.6)$ Å scaled according to location relative to the bilayer center. Figure 4(b) shows the changes in the positions of the methylene, double-bond, carbonyl, glycerol, and water moieties relative to the positions in the peptide-free bilayer for bilayer model A. A nominal uncertainty in position of ± 0.5 Å is indicated by the horizontal error bar centered on the glycerol position.

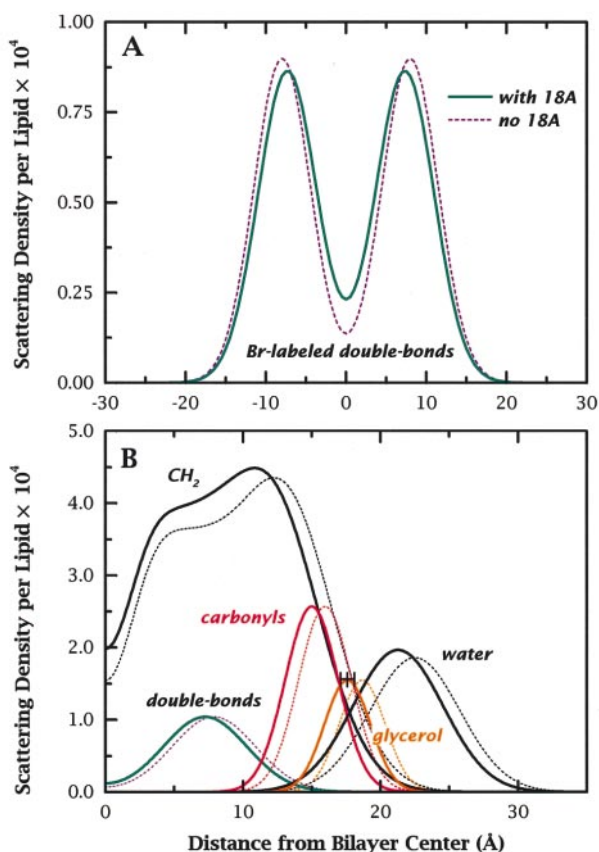


Figure 4. Comparisons of the transbilayer distribution of Br labels on OBPC double bonds and of selected quasimolecular fragments of DOPC bilayers obtained in the absence and presence of Ac-18A-NH₂. (a) The experimentally determined transbilayer distribution of the Br-labeled double bonds of OBPC/DOPC bilayers shows the effect of Ac-18A-NH₂ (18A) on the double-bond distribution and hence the structure of the HC core of the bilayer. The peptide causes the HC core to thin slightly, as shown by the shift of the Br peak toward the bilayer center by 0.65 Å. Because this change is small, a model for the structure of the perturbed bilayer can be constructed (see the text). (b) Comparison of the structures of DOPC bilayers in the absence and presence of 18A. The perturbed structure (continuous curves) is obtained from the unperturbed structure (dotted curves) by a simple scaling procedure (see the text). The unperturbed structure is that described by Wiener & White (1992b). The perturbed structure is that of model bilayer A (see the text). A nominal uncertainty in position of ± 0.5 Å is indicated by the horizontal error bar centered on the glycerol position (see the text).

Step 3: best-fit Gaussian transbilayer distributions of Ac-18A-NH₂

We determined the positions $\pm Z_p$ and 1/e-half-width A_p of the optimal Gaussian pairs for the transbilayer peptide distributions that satisfied the experimentally determined structure factors as described in Materials and Methods. Experimental uncertainties of the distributions were determined

Table 2. Bragg spacings and Gaussian parameters ($\text{\AA} \pm \text{s.d.}$) for the transbilayer distribution of the double-bond bromine labels of OBPC in DOPC/OBPC oriented multilayers bilayers without and with Ac-18A-NH₂ (18A)

Parameter	DOPC/OBPC ^a	DOPC/OBPC + 18A
d^b	49.1 ± 0.30	46.5 ± 0.50
Z_{Br}^c	7.97 ± 0.27	7.32 ± 0.12
A_{Br}^d	4.96 ± 0.62	5.16 ± 0.87

^a Data from Wiener & White (1991c).

^b Bragg spacing.

^c Position of Gaussian.

^d 1/e-halfwidth of Gaussian.

using the Monte Carlo method described by Wiener & White (1992b). For bilayer model A, $A_p = 17.19(\pm 0.22)$ \AA and $A_p = 4.32(\pm 0.19)$ \AA . For bilayer model B, $Z_p = 16.98(\pm 0.26)$ \AA and $A_p = 4.63(\pm 0.22)$ \AA . Student's *t*-test showed that these Gaussian parameters are not statistically different for the two models. We therefore took the average values of Z_p and A_p from the two models as the best estimates for the parameters: $Z_p = 17.1(\pm 0.3)$ \AA and $A_p = 4.5(\pm 0.3)$ \AA .

The four-order reconstructions of the membrane profiles resulting from the refinement are summarized and compared in Figure 5. Shown for bilayer models A and B are the profiles for Ac-18A-NH₂ (violet curves), the bilayer model (blue curves), and the bilayer model + Ac-18A-NH₂ (red curves). The bilayer/Ac-18A-NH₂ curves fall within the error limits of the experimentally observed bilayer/Ac-18A-NH₂ profile (pairs of black curves), demonstrating graphically the excellent agreement of the models with the experimental data.

Step 4: modeling the peptide conformation, position, and orientation

The most realistic approach to modeling the peptide would be to produce an ensemble of conformations in a bilayer environment by molecular dynamics simulations, but this approach is presently impractical. We therefore adopted a simpler method that allowed us to explore a reasonable range of peptide backbone and side-chain conformations. For a particular peptide conformation, each atom (*a*) was represented in the *z*-axis projection by a Gaussian scattering distribution whose 1/e-halfwidth A_a was related to the atom's *B*-factor (see Materials and Methods). All atoms were assigned the same *B*-factor during the refinement procedure.

The structure refinement for a particular backbone conformation began with the construction of an axis along the mean center of mass of the model. For a given orientation of this axis relative to the bilayer plane, the scattering distributions of the atoms were then projected onto the *z*-axis and added together to obtain the total scattering distribution of the peptide model. Because the diffraction experiment is one-dimensional, all orientations of the peptide obtained by precession of the peptide axis around the *z*-axis are equivalent. Thus, the distribution of the atoms projected onto the *z*-axis will be affected only by the tilt angle γ of the peptide axis relative to the bilayer plane, the position of the center of the peptide axis along the bilayer normal, and the rotation of the peptide around its axis (rotation angle $\equiv \eta$). In the refinement protocol, we explored primarily the position, tilt angle, and *B*-factors of the atoms.

We created molecular models of Ac-18A-NH₂ with the software package Insight II (Biosym, Technologies, San Diego, CA), as discussed in Materials

Table 3. Positions (*Z*) and 1/e-halfwidths (*A*) of the Gaussian distributions in \AA of the quasimolecular fragments of DOPC bilayers in the absence and presence of Ac-18A-NH₂

Fragment ^a	DOPC	DOPC	DOPC + 18A	DOPC + 18A
	<i>Z</i> ^b	<i>A</i> ^b	model A <i>Z</i> ^c	model B <i>Z</i> ^c
CH3	0 ^a	2.95	0	0
iCH2	2.97	2.74	2.73	2.81
mCH2	5.86	4.21	5.39	5.55
oCH2	12.85	5.14	11.82	12.17
CC	7.88	4.29	7.25	7.46
COO	15.97	2.73	15.00	15.12
GLYC	18.67	2.37	17.59	17.68
PO4	20.19	3.08	19.05	19.12
CHOL	21.89	3.48	20.68	20.73
WATER	22.51	4.63	21.28	21.32

^a Nomenclature is that of Wiener & White (1992b). CH3, terminal methyl groups; CC, double-bonds; COO, carbonyl groups; GLYC, glycerol group; PO4, phosphate group; CHOL, choline group. The methylene (CH2) group distribution is described by three Gaussians (i, inner; m, middle; o, outer).

^b Data taken from Wiener & White (1992b).

^c Approximate uncertainties in these positions can be estimated from the experimental uncertainties of the peptide-induced changes in bromine-label position ΔZ_{Br} (± 0.30 \AA) and Bragg spacing $\Delta d/2$ (± 0.6 \AA) scaled according to location relative to the bilayer center.

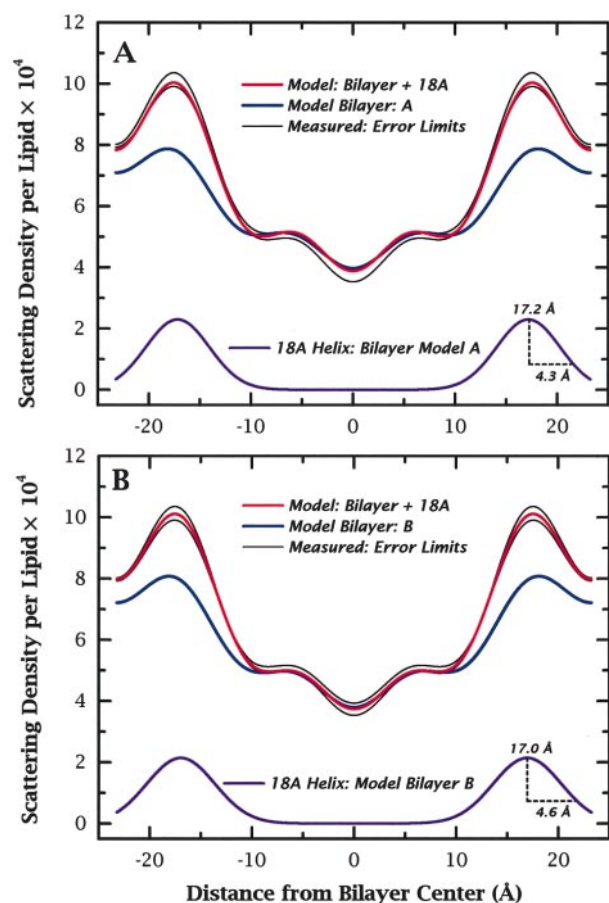


Figure 5. Scattering density profiles summarizing the results of the absolute-scale refinement of the structure of a fluid DOPC bilayer containing α -helical Ac-18A-NH₂ in the interface aligned approximately parallel with the bilayer plane. To arrive at the Fourier reconstructions shown by continuous red curves, the computed structure factors of the model bilayers (continuous blue curves) are added to the structure factors of Ac-18A-NH₂ computed from the Gaussian fits (continuous violet curves) such as those shown in Figure 7. The computed profiles of DOPC/Ac-18A-NH₂ fall within the error limits of the observed profiles (continuous black curves). (a) Profiles computed for model bilayer A. The long axis of the helix is found to be located at 17.2 Å. (b) Profiles computed for model bilayer B. In the case, the helix axis is located at 17.0 Å. The two positions agree within experimental uncertainty. The mean position is 17.1(\pm 0.3) Å.

and Methods. Many model structures were constructed, but a large number of them could be caused to fit the experimental data through appropriate combinations of peptide position, helix tilt angle, and atomic B -factor. Therefore, only four structures, defined by the backbone (BB) Φ , Ψ angles, are presented here for illustrative purposes. BB Model I _{α} had an ideal helix conformation with $\Phi = -65^\circ$ and $\Psi = -40^\circ$. BB model II _{α} was produced from model I _{α} through a 5 ps molecular dynamics (MD) run performed at 300 K. Similarly, BB model III _{α} was produced by a 5 ps MD simu-

lation at 500 K. We also created a fully extended chain conformation, BB model IV_{ex}. The backbone conformations and Φ , Ψ angles for BB models I _{α} , II _{α} , and III _{α} are shown in Figure 6.

Structure refinement

For a particular combination of peptide model and model bilayer, the refinement computation finds the optimal position and B -factor of the peptide model. For each cycle of the computation, the computed structure factors of the peptide atoms are added to the fixed structure factors of the bilayer model, and these computed structure factors compared to the observed structure factors of the DOPC/Ac-18A-NH₂ complex by means of the crystallographic R -factor. The computation involves non-linear minimization of R using the standard Levenberg-Marquardt algorithm (Bevington, 1969; Press *et al.*, 1989) in order to obtain the optimal B -factor and Z_p . The 1/e-half-width A_p of the transbilayer peptide distribution is obtained from the envelope of the summed atomic

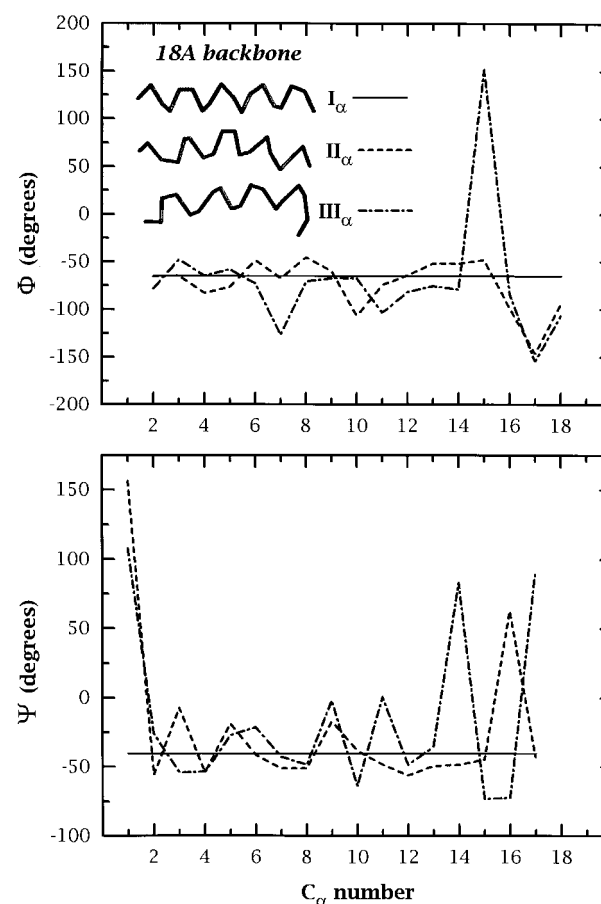


Figure 6. Plot of the dihedral (Φ , Ψ) angles versus C_α number for the three helical peptide models used in the absolute-scale refinement of the structure of DOPC bilayers containing Ac-18-NH₂. The insets show molecular graphics images of the backbone conformations matching the Φ , Ψ angles.

Gaussians. Only those solutions are accepted whose R -factors are smaller than the so-called "self" R (R_{self}) of the observed structure factors. R_{self} measures, in essence, the total experimental uncertainty of the observed structure factors after scaling (Wiener & White, 1991a; and see Materials and Methods). The value of R_{self} was 6.35×10^{-2} for the experiments reported here.

Refinement results and selection of most likely Ac-18A-NH₂ models

Refinements were performed for each of the four peptide models in each of the two bilayer models. For each combination of model peptide and bilayer model, minimizations were carried out for a series of peptide tilt angles γ and rotation angles η .

Table 4. Mean positions (Z_p), 1/e-halfwidths (A_p), thermal B -factors, and R -factors determined from fits to the experimental structure factors (Table 1) for the three helix backbone (BB) conformations (BB models I_α, II_α, and III_α) shown in Figure 6 and an extended chain (BB model IV_{ex}).

BB model	Z_p (Å) ^a	A_p (Å) ^b	B (Å ²) ^c	$R \times 10^{2d}$
A. Model bilayer A^e				
I _α ^{η₁}	16.99	4.40	418.3	5.6
I _α ^{η₂}	17.37	4.39	416.9	5.7
II _α ^{η₁}	17.06	4.43	126.5	5.3
II _α ^{η₂}	17.31	4.41	120.9	5.6
III _α ^{η₁}	17.12	4.79	56.6	5.1
III _α ^{η₂}	17.30	4.79	54.0	5.2
IV _{ex} ^{η₁}	17.28	4.29	451.8	6.3
IV _{ex} ^{η₂}	17.10	4.29	451.5	6.3
B. Model bilayer B^e				
I _α ^{η₁}	16.61	4.82	570.1	1.9
I _α ^{η₂}	17.14	4.87	528.8	0.45
II _α ^{η₁}	16.84	4.74	241.6	1.0
II _α ^{η₂}	16.94	4.87	292.1	1.9
III _α ^{η₁}	16.90	4.99	179.9	1.6
III _α ^{η₂}	17.07	4.98	179.1	1.3
IV _{ex} ^{η₁}	17.06	4.62	563.5	0.63
IV _{ex} ^{η₂}	16.88	4.62	563.1	0.62

Peptide models were constructed using the software package Insight II as described in Materials and Methods. The long axis of the peptide models are parallel with the bilayer plane ($\gamma = 0^\circ$, Figure 8). For each model, two rotational positions around the long axis are shown ($\eta_1 = 0^\circ$ and $\eta_2 = \eta_1 + 180^\circ$).

^a Center of the transbilayer distribution of Ac-18A-NH₂ in DOPC bilayers defined as the mean of the atom coordinates of the model. It is generally different from the center of scattering because scattering weights positions according to atomic scattering lengths.

^b The 1/e-halfwidth of the envelope of the distribution defined by the sum of the Gaussian distributions of the individual atoms.

^c The crystallographic thermal B -factor is related to the 1/e-halfwidth A_a of an atom's Gaussian distribution through $B = 4\pi^2 A_a^2$ with $A_a^2 = A_c^2 + A_l^2$, where A_c is the atom's covalent radius. For comparison, the B -factors for some of the lipid's interfacial quasimolecular fragments (Table 3) are $B_{\text{COO}} = 123.43$, $B_{\text{glyc}} = 71.38$, $B_{\text{chol}} = 219.77$, $B_{\text{PO4}} = 203.7 \text{ \AA}^2$.

^d R -factor, defined as $R = \frac{\sum_h ||\bar{F}^*(h)|| - |F_m(h)|}{\sum_h ||\bar{F}^*(h)||}$, where F_m are the structure factors of the DOPC/Ac-18A-NH₂ model (see Table 1). The values of R are of the order of, or smaller than, the value of the self R -factor ($R_{\text{self}} = 6.3 \times 10^{-2}$, see the text).

^e Described in Table 3.

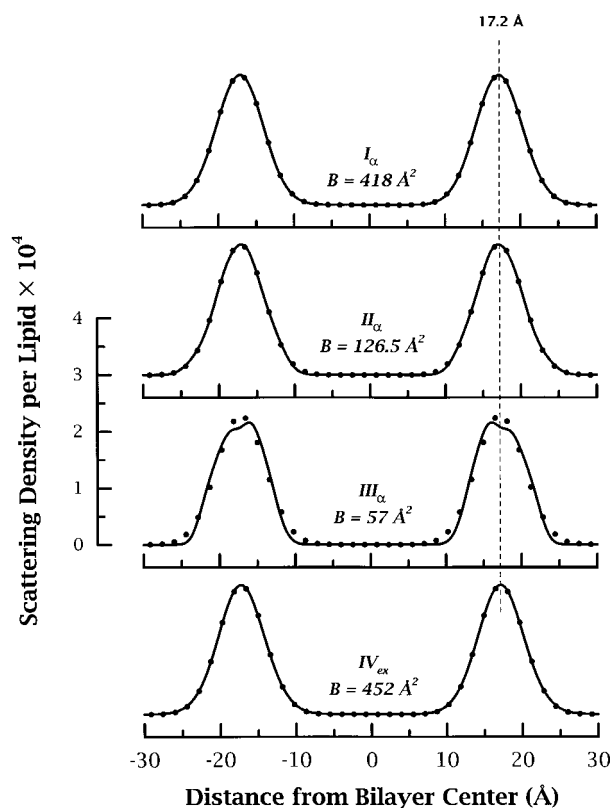


Figure 7. Scattering density profiles of the four model structures of Ac-18A-NH₂ in DOPC bilayers resulting from the absolute-scale refinement using model bilayer A as the structure of the perturbed bilayer. The continuous lines show the profiles that result from summing the thermal envelopes of the atoms of the peptides (see the text). The superimposed dots indicate the results of fitting Gaussian curves to the profiles. The refinement procedure finds the optimal position of the centers of scattering of the peptides and their average atomic B -factors. For the curves shown, the long axis of the peptide models were aligned parallel with the bilayer plane. The maxima of all curves occur at the same distance from the bilayer center. Notice, however, that the B -factors of the peptide models differ dramatically. The values shown should be considered in the context of the range of B -factors, 70-200 \AA^2 , observed for the interfacial quasimolecular fragments of the fluid DOPC bilayer (see the text). Notice that the continuous curve for BB model III_α has two local maxima. This is a result of its contorted backbone (BB) conformation (see Figure 6).

Typical results for bilayer models A and B and peptide BB models I_α, II_α, III_α, and IV_{ex} with $\gamma = 0^\circ$ are summarized in Table 4. Examples of the scattering-density profiles for each of the model peptides in bilayer model A (Table 4) obtained by summing the atomic Gaussians are presented in Figure 7 as continuous curves. Superimposed on these curves as dots are the fits of single Gaussians to the summed atomic Gaussians. As expected, a summed-Gaussian envelope can generally be described accurately by a single Gaussian function.

Three observations about Table 4 and Figure 7 are important. First, both helical and extended-chain peptide models provided satisfactory fits to the experimental data, but with dramatically different B -factors. Second, all of the transbilayer peptide distributions for particular model bilayers and model peptides yielded the same position for the Gaussian peak, as illustrated in Figure 7 for $\gamma = 0$. This reveals the robustness of the fits and further justifies using single Gaussians in step 3. Third, the B -factors required for a good fit to the experimental data, ranging from 57 to 570 \AA^2 (Table 4 and Figure 7), depend strongly on the backbone conformation of the model peptide. In general, the tighter the conformation of the backbone and side-chains, the larger the B -factor must be in order to obtain a satisfactory fit. The B -factors obtained are huge by protein crystallographic standards; B -factors for high-resolution protein structures are typically $\sim 25 \text{\AA}^2$. The reasonableness of the B -factors obtained must be judged against the apparent B -factors of the quasimolecular groups of the fluid bilayer interface that range from 70 \AA^2 for the glycerol group to about 200 \AA^2 for the choline and phosphate groups. Because the thermal motion of the peptide must be tightly coupled to the thermal motion of the bilayer, reasonable peptide B -factors should fall within this range. By this criterion, the most reasonable models are BB model II _{α} in model bilayer A and BB model III _{α} in model bilayer B (Table 4 and Figure 7).

The B -factors also depend, however, on the peptide tilt angle, as shown in Figure 8 for the helical peptide models in model bilayer A. As expected,

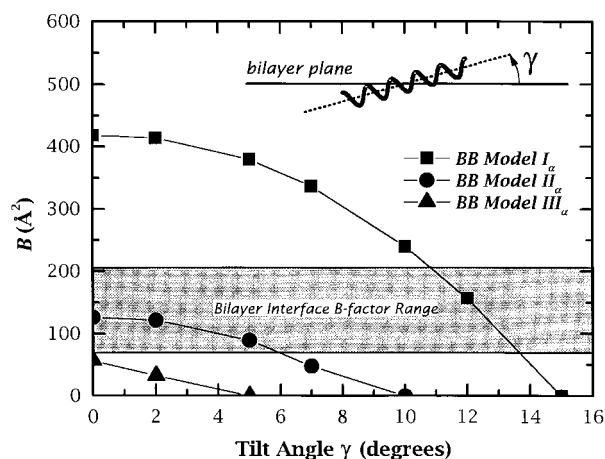


Figure 8. The effect of helix orientation on the B -factors required to achieve a satisfactory refinement for the three helical peptide models. The larger the tilt angle, the smaller B must be in order for a satisfactory fit to the experimental data to be obtained. The shaded area delineates the range of B -factors expected, based upon the known B -factors of the interfacial quasimolecular fragments of fluid DOPC bilayers. These data suggest that BB models II _{α} and III _{α} are the most reasonable representations of helical Ac-18A-NH₂ structures, but in any case, the data show that the long axis of helical conformations must be tilted no more than about 10–15°.

the greater the tilt angle, the smaller the B -factor has to be in order to achieve a satisfactory fit to the experimental data. The range of bilayer interface B -factors, shown by the shaded area of Figure 8, suggested conformations and tilt angles that could be reasonably expected for the helices in the bilayer. The perfect helix, BB model I _{α} , is reasonable provided γ is between 10° and 14°, whereas BB model III _{α} is reasonable only for $\gamma = 0^\circ$. The moderately disordered helix, BB model II _{α} , can be accommodated with a γ of 0–6°. We therefore concluded that Ac-18A-NH₂ is helical with $\gamma < 14^\circ$. The thermal motion of the bilayer, however, makes it seem unlikely that the backbone would be a perfect helix or that γ would be rightly constrained. These considerations suggest that BB model II _{α} with γ fluctuating between 0° and 6° is the most reasonable description of Ac-18A-NH₂ in DOPC bilayers under the conditions of our experiments.

Evaluation of the structure refinement

The validity of the absolute-scale refinement results is supported by four lines of evidence. First, the overall quality of the diffraction data can be judged by considering whether the observed effects of the peptide on the diffracted X-ray intensities are sensible. In X-ray diffraction studies of pure DOPC bilayers, seven or eight diffraction orders were observed (Wiener & White, 1991c, 1992b). When Ac-18A-NH₂ was present, however, we could observe only four or five orders of diffraction, depending upon the mol% of OPBC. There are two possibilities for this effect: either five orders of diffraction were sufficient for describing the fully resolved profile, or poor experimental technique prevented observation of higher orders. To distinguish between these possibilities, we calculated the structure factors of the bilayer/Ac-18A-NH₂ models out to $h = 8$. The results of the calculations are presented in Table 1, where it is seen that structure factors for $h > 5$ are small, but non-zero. Could they have been observed in a carefully performed experiment? The answer depends, of course, upon the signal-to-noise ratio of the experiment in which one observes intensities $I_h = F_h^2/h$. In order to examine the observability of the diffracted intensities, we calculated expected values of I_h taking I_1 arbitrarily as equal to 1000. The results of the calculation are presented in Table 5. Included for comparison are values of I_h calculated for pure DOPC bilayers from the data of Wiener & White (1991c), who could observe no more than eight diffraction orders, even with extremely long exposures. Orders 6, 7, and 8 were near the signal-to-noise limit in their experiments. The data of Table 5 indicate that for DOPC bilayers containing Ac-18A-NH₂, the expected values of orders 6, 7, and 8 are typically about an order of magnitude smaller than those observed for pure DOPC. Furthermore, the calculated values of these orders never exceed the second order of pure DOPC, which is not easily observed even for

Table 5. Experimental and computed diffracted intensities $I(h)$ normalized to make $I(1) = 1000$

h^a	DOPC + 18A (observed)	DOPC + 18A with model bilayer A ^b	DOPC + 18A with model bilayer B ^b	DOPC alone (computed) ^c
1	1000	1000	1000	1000
2	0.28	0.014	0.23	0.055
3	22.40	24.63	23.31	4.85
4	21.03	25.19	19.86	18.56
5	0.58	1.77	1.08	1.31
6	n.o. ^d	(0.11)	(0.075)	0.58
7	n.o. ^d	(0.024)	(0.021)	0.29
8	n.o. ^d	(0.033)	(0.041)	0.24

Intensities are calculated from model structure factors $F_m(h)$ using $I(h) = F_m(h)^2/h$.

^a Diffraction order.

^b Computed using the structure factors $F_m(h)$ from Table 1.

^c Computed with model structure factors $F_m(h)$ by Wiener & White (1991c).

^d Not observable.

highly oriented samples at 66% RH. Therefore, the high orders of diffraction were not expected to be observable, and in fact were not. We conclude that when the helix is present in the bilayer it causes a smoother profile and effectively “dampens” the high-order structure factors, causing a maximum of only five orders of diffraction to be sufficient for full resolution of the profile. That is, the broad distribution of the thermally disordered Ac-18A-NH₂ helix masks the finer detail of the fluid bilayer itself.

Second, the quality of the refinement can be judged by considering the agreement between the model-independent real-space distribution determined in step 1 and bilayer-model-dependent Gaussian distribution determined in step 3. The real-space difference structure of step 1 suggested a Gaussian-like distribution centered at $Z_p = \pm 16.6$ Å with a full-width of about 10 Å (Figure 3), while the best-fit Gaussian distribution of step 3 had parameters $Z_p = \pm 17.1(\pm 0.3)$ Å and 1/e-half-width $A_p = 4.5(\pm 0.3)$ Å. The agreement between these distributions is well within the $\delta d/2 \sim 1$ Å uncertainty of the real-space difference structure that arises primarily from the change in Bragg spacing caused by the peptide (see above). The widths of both distributions are consistent with crystallographic observations on the helices of helix-bundle membrane proteins. The mean diameter D_{hlx} of a helix in the bilayer can be estimated from $D_{\text{hlx}} \approx 2A_p$ to be about $9(\pm 0.6)$ Å. This compares quite favorably with the average center-to-center spacing of $9.6(\pm 1.9)$ Å observed for 45 transmembrane helices in membrane proteins of known structure (Bowie, 1997). These considerations alone strongly suggest that Ac-18A-NH₂ in the bilayer exists as an α -helix lying parallel with the bilayer surface.

Third, the agreement between these two peptide distributions provides support for the bilayer models developed in step 2. The need for the models is clear from the decrease in Bragg spacing and the inward shift of the Br-labeled double bonds caused by the peptide. Furthermore, the simple expedient of using the neat DOPC bilayer

structure in step 3 failed on two counts, primarily because of the incorrect Bragg spacing: large structure factors were obtained in the refinement for $h = 6, 7,$ and $8,$ and R -factors significantly greater than R_{self} were obtained. The very small inward shift of the double bonds with virtually no change in width suggests that the models are likely to be very good approximations of the perturbed bilayer structure. This is supported by the fact that the two bilayer models used led to statistically equivalent peptide distributions in step 3 that are very close to real-space difference-structure distribution determined in step 1. The strongest overall evidence for the models is the quality of the agreement between the observed structure factors and those computed from the bilayer models (Table 1 and Figure 5). The model structure factors agree with the observed ones well within the accumulated experimental error described by R_{self} .

Finally, the quality of the peptide models in step 4 was tested in two ways. The first test was the internal consistency of the refinement procedure. Good consistency was indicated by the excellent agreement between the peptide distributions determined in steps 3 and 4 (Table 4, Figures 5 and 7). The second, and much more important, test was the direct observation of the conformation and orientation of Ac-18A-NH₂ in DOPC bilayers using oriented circular dichroism under experimental conditions identical with those of the diffraction experiments (see Materials and Methods). The oriented CD spectrum shown in Figure 9 for 5 mol% Ac-18A-NH₂ is an average over eight different azimuthal angles obtained at 66% RH. The data show unambiguously that the peptide conformation was predominantly α -helical in our experiments, about 80% as estimated from the ellipticity value at 222 nm. Furthermore, the shape of the spectrum indicates that the peptide was oriented perpendicular to the beam and parallel with the bilayer surface (Wu *et al.*, 1990). These CD data suggest that BB model II _{α} with $\gamma < 6^\circ$ is a reasonable description of Ac-18A-NH₂ in the fluid DOPC bilayer at 66% RH.

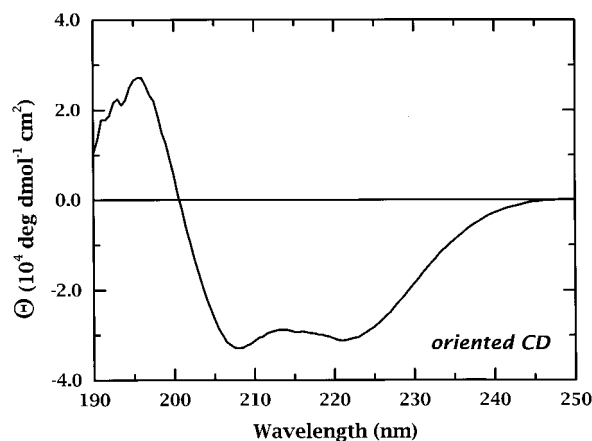


Figure 9. Oriented circular dichroism spectrum for Ac-18A-NH₂ (5 mol%) in oriented DOPC bilayers at 66% RH collected under the same conditions as the diffraction experiments. The samples were prepared as in the diffraction experiments using quartz slides that were placed in the spectropolarimeter normal to the optical path. The data show that the peptide conformation is predominantly α -helical, about 80% based upon its ellipticity value at 222 nm. The shape of the spectrum indicates that the peptide is oriented perpendicular to the optical path and parallel with the bilayer surface, based upon the theory and observations reported by Wu *et al.* (1990). These data are entirely consistent with BB models II _{α} and III _{α} being reasonable examples of the conformations of Ac-18A-NH₂ in the bilayer.

Discussion

The results presented above provide the first view of the structure of an amphipathic α -helix in a fluid lipid bilayer determined by absolute-scale refinement. The incorporation of 5 mol% of Ac-18A-NH₂ into DOPC bilayers at 66% RH caused the Bragg spacing to decrease from 49.1 Å to 46.5 Å (Table 2) and the double bonds to shift towards the bilayer center by 0.65 Å (Table 2, Figures 2 and 4(a)). These changes indicate that the peptide caused the bilayer to thin slightly, as observed in diffraction studies on other peptide/bilayer systems (Jacobs & White, 1989; Wu *et al.*, 1995). The absolute-scale refinement allowed us to establish that the transbilayer distribution of the peptide can be described by a Gaussian located at $Z_p = 17.1(\pm 0.3)$ Å from the bilayer center with an $1/e$ -halfwidth $A_p = 4.5(\pm 0.3)$ Å (Figure 5), consistent with the center-to-center helix packing of 9.6(± 1.6) Å observed in helix-bundle membrane proteins (Bowie, 1997). The refinement procedure yielded the optimal positions and average atomic B -factors of several peptide models (Figure 7). Overall, the analysis suggested that a somewhat disordered helix, such as BB model II _{α} or III _{α} , with $\gamma < 6^\circ$ was an appropriate description of the average conformation of the peptide. Oriented circular dichroism measurements of Ac-18A-NH₂ in DOPC bilayers (Figure 9), made under the same experimental conditions as the diffraction measure-

ments, were entirely consistent with these modeling results.

We can therefore conclude, with considerable confidence, that Ac-18A-NH₂ is highly helical, oriented approximately parallel with the bilayer plane, and located 17.1(± 0.3) Å from the bilayer plane. As shown in Figure 10, this places the helix axis close to the average position of the glycerol groups of the DOPC bilayer. Based upon the width of the Ac-18A-NH₂ Gaussian distribution, Figure 10 also shows that the thermally disordered surface of the helix extends approximately to the depth of the DOPC double bonds. This penetration into the HC core is somewhat deeper than proposed by Clayton & Sawyer (1999) based upon fluorescence measurements. The surface of the helix facing the HC core is presumably the non-polar surface, as suggested in Figure 10, but we have no direct proof that that is the case. The refinement studies show that rotations of the helices about their axes have only minor effects on the quality of the fits of the model structure factors to the experimental data (Table 4). The broad thermal width of the helix makes it impossible to determine the exact locations of the different amino acid residues. Neutron diffraction and specific deuterium labeling will be required for such determinations. We were surprised that it was possible to form highly oriented and strongly diffracting lamellar arrays of Ac-18A-NH₂/DOPC bilayers, because the peptide is so highly charged and no counter-ions were present in the system. We can only presume that some combination of lysine deprotonation, aspartate/glutamate protonation, Coulombic interactions with headgroups, and intrahelical salt-bridge pairing (Lund-Katz *et al.*, 1995) occurs.

The so-called snorkel hypothesis (Segrest *et al.*, 1990) has been proposed to explain the presence of basic amino acid residues at the polar/non-polar interface and acidic amino acid residues in the center of the polar face of class A amphipathic helices such as Ac-18A-NH₂ (Mishra *et al.*, 1994). The hypothesis proposes that the amphipathic character of the basic residues, especially lysine, causes them to extend toward the polar face of the helix in order to insert their charged moieties into the interfacial aqueous region so that their non-polar van der Waals surface can contact the HC core. The computer program LAMBDA (Lipid Affinity Measured By Depth Algorithm, Palgunachari *et al.*, 1996), based in part upon this hypothesis, predicts that the center of the Ac-18A-NH₂ helix axis will be located 4-5 Å beneath the lipid phosphate group with a tilt angle of 4.6° and will penetrate to within 8-9 Å of the center of the HC core. The data presented here agree approximately with these predictions (see Figure 10). However, this agreement for a single example of a class A helix may be fortuitous and cannot, therefore, be considered as a general test of the snorkel hypothesis.

The X-ray diffraction and circular dichroism experiments provide only one-dimensional information about the disposition of Ac-18A-NH₂ in the

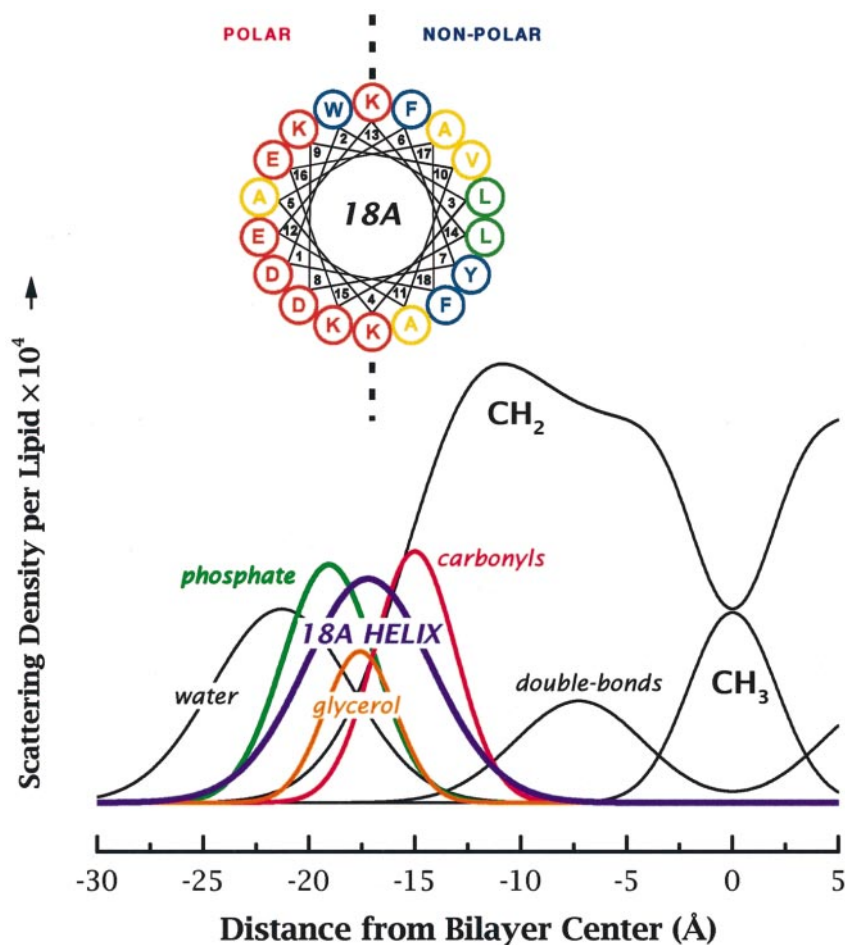


Figure 10. Summary of the results of the structural refinement of Ac-18A-NH₂ in DOPC bilayers showing the trans-bilayer distribution of the α -helix in the context of the structure of the fluid DOPC bilayer. The inset shows a helical-wheel representation of the Ac-18A-NH₂ aligned parallel with the bilayer plane with the non-polar surface facing the HC core of the bilayer (not to scale). The Gaussian distribution of the helix indicates that the thermally disordered surface of the helix penetrates the HC core to the level of the double bonds. The helix axis located 17.1 Å from the bilayer center coincides closely with the mean position of the DOPC glycerol groups located about 17.6 Å from the center. The amino acids of the helical wheel are color-coded according to the interfacial hydrophobicity scale established by Wimley & White (1996). On that scale, partitioning of aromatic residues (blue) is highly favorable, leucine moderately favorable (green), alanine and valine slightly favorable (yellow), and all charged residues highly, but about equally, unfavorable (red). Ideally amphipathic Ac-18A-NH₂ resides precisely at the headgroup/HC core boundary as is often assumed, but never previously demonstrated directly.

bilayer. What can be said about its disposition in the other two dimensions? Simple geometric considerations, summarized in Figure 11, can be used to address two basic questions: the area density of helices in the bilayer plane and the packing of the lipids around the helices. Treating Ac-18A-NH₂ as a helix 27 Å long with a diameter of 10 Å, its projected surface area on the bilayer plane is ~ 270 Å² compared to the total surface area of ~ 1200 Å² for its associated 19 lipid molecules that each occupy ~ 60 Å². Although the helices are not tightly packed in the membrane plane, as shown schematically in Figure 11(a), they nevertheless have a significant effect on the ways that the lipids can occupy volume and area in the bilayer. This is immediately apparent from the changes in Bragg spacing d and lipid hydration induced by Ac-18A-NH₂. Because d decreases without a major change

in lipid hydration, the helices must at least cause the area per lipid S to increase. But, the following calculations show that the helices also contribute independently to the area of the interface. Consider first pure DOPC bilayers at 66% RH. The molecular volume of DOPC is 1295 Å³ (Wiener & White, 1992a) and the volume of its 5.4 water molecules of hydration is 162 Å³. Because ideal volumetric mixing appears to prevail in fluid bilayers at low hydration (White *et al.*, 1987), the Bragg spacing of 49.1 Å leads to $S = 59.3$ Å² (Wiener & White, 1992a). When Ac-18A-NH₂ is present, the hydration increases to 5.7 water molecules per lipid molecule and the Bragg spacing decreases to 46.5 Å, indicating that S must increase slightly, as expected, to 63.0 Å². But, the situation is actually more complicated. A half-unit cell of the peptide/DOPC membrane contains 1/19 of a peptide as

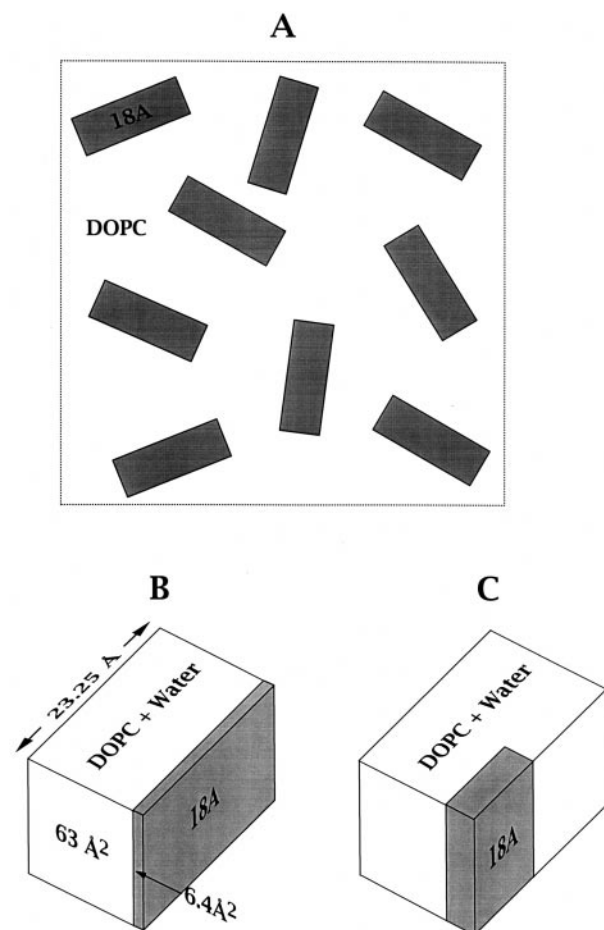


Figure 11. Representations of the distribution of Ac-18A-NH₂ on the surface of the DOPC bilayer and of the packing of DOPC, water, and Ac-18A-NH₂ in a half-unit cell of the membrane. (a) A plan view of Ac-18A-NH₂ helices distributed on the surface of a DOPC bilayer constructed so the projected area of a helix is 270 Å² and the area of its associated 19 lipid molecules is about 1200 Å². (b) A summary of the contributions of DOPC + water and of Ac-18A-NH₂ to the cross-sectional area of the half-unit cell, computed as follows. The half-unit cell contains 1 DOPC, 5.7 water molecules, and 1/19 of an Ac-18A-NH₂ whose volumes are, respectively, 1295 Å³ (Wiener & White, 1992b), 171 Å³, and 147 Å³. The molecular volume of a water molecule is 30 Å³ and the volume of a whole peptide is 2800 Å³, calculated from the amino acid partial molar volumes determined by Makhatadze *et al.* (1990). Given $d/2 = 23.25$ Å and the half-unit cell volume of 1613 Å³, the cross-sectional area of the unit cell is 69.37 Å². Of this total, DOPC + water contributes 63.05 Å² and Ac-18A-NH₂ 6.32 Å². (c) An illustration showing that, at constant half-unit cell volume, the volumes of the peptide and lipid can be rearranged to allow only partial penetration of the bilayer by the peptide.

well as the water and the DOPC molecule. We estimate from the data presented by Makhatadze *et al.* (1990) that the volume of Ac-18A-NH₂ is about 2800 Å³, which means that the volume of peptide in the half-unit cell is about 147 Å³. The total

volume of the half-unit cell and the Bragg spacing lead to a cross-sectional area of the half-unit cell of 69.4 Å², meaning that Ac-18A-NH₂ contributes an additional interfacial area of about 6.4 Å² per lipid molecule. Figure 11 shows how these numbers can be reconciled with one another. Figure 11(b) summarizes the per-lipid contributions of Ac-18A-NH₂ to half-unit cell volume and interfacial area. Figure 11(c) shows one of the many ways that the lipid and peptide volumes can be isovolumetrically redistributed in order to accommodate the partial penetration of Ac-18A-NH₂ into the bilayer. In the case shown, the headgroups occupy slightly less area and the terminal methyl groups slightly more. These simple images show that the packing of the helix and the lipid in membrane is entirely consistent with the helix being embedded in the bilayer interface. Because we have shown that the bilayer structure is not strongly perturbed by the peptide, it appears that the lipids can adapt readily to the surface of the helix.

Our results encourage us to believe that the absolute-scale refinement approach will be generally useful for understanding the structural consequences of the interactions of a wide range of peptides and proteins with lipid bilayers. It should be especially useful for testing predictions of the depth and orientation of amphipathic helices in membranes (Segrest *et al.*, 1974; Brasseur *et al.*, 1988; Brasseur, 1991; Jones *et al.*, 1992; Palgunachari *et al.*, 1996). Its main shortcoming at present is that it can be applied to DOPC bilayers only at low levels of hydration. However, recent advances in sample preparation and orientation (Katsaras, 1997, 1998) suggest that the method can eventually be extended to fully hydrated bilayer systems. When combined with thermodynamic measurements, the added structural information should provide a better basis for quantitative descriptions of peptide-bilayer interactions at the molecular level. Finally, the method raises the possibility of combining diffraction results with molecular dynamics simulations of peptides in bilayers, which are becoming increasingly feasible as computer speeds increase (Huang & Loew, 1995; Bernèche *et al.*, 1998).

Materials and Methods

Materials and sample preparation

DOPC and OBPC were purchased from Avanti Polar Lipids (Alabaster, AL). The purity of OBPC was determined by elemental analysis to be better than 99.9% (Microlit Laboratories, Madison, NJ). Ac-18A-NH₂ was synthesized and purified as described (Venkatachalapathi *et al.*, 1993).

Lipid/peptide multilayers were deposited on a curved glass surface as described (Wiener & White, 1991c; Hristova & White, 1998). The relative humidity (RH) was maintained at 66% with a saturated solution of NaNO₂. The sample was placed in a custom-made humidity chamber with two thin X-ray transparent beryllium windows. The sample was adjusted in the

chamber such that the incident X-rays were tangent to the curved surface of the oriented multilayer at a glancing angle so that all of the lamellar diffraction orders were recorded in a single experiment. In this geometry, much of the wide-angle diffraction due to lipid acyl chains is absorbed by the glass substrate (Wiener & White, 1991c). Sample degradation was monitored by TLC and HPLC. No degradation of irradiated samples was observed over periods of one to two days, which is long compared to typical X-ray exposure times of eight to ten hours. Furthermore, no systematic differences in the line-widths or integrated intensities were observed.

Determination of sample hydration

The weight of a volumetric flask was measured in vacuum and in a 66% RH environment. Ten mg of DOPC dissolved in chloroform was added to the flask. The chloroform was evaporated under a stream of nitrogen, and the flask placed under vacuum in the presence of NaOH. Following equilibration, its weight was determined. The flask was then transferred into a sealed container containing a saturated solution of NaNO₂ in order to achieve equilibration at 66% RH in order to verify equilibrium hydration of the sample at the known (White *et al.*, 1987) level of 5.4 water molecules/lipid molecule. Ac-18A-NH₂, 1.44 mg dissolved in MeOH, was added to the lipid. After the lipid was dissolved in the MeOH, the solvent was evaporated, and the mixture was desiccated/hydrated several times. The difference in the weight of the hydrated and desiccated lipid/peptide mixture, corrected for the difference in the weight of the hydrated and desiccated flask gave the weight of the hydrating water.

Oriented circular dichroism

Oriented CD measurements were performed using a modified version of the method of Wu *et al.* (1990). DOPC and Ac-18A-NH₂ were co-dissolved in methanol. Dropwise, the methanol solution was deposited on a quartz slide to form a spot with a 1 cm diameter, and the methanol removed under vacuum. The quartz slide was glued to a custom-designed tube with a quartz bottom, containing a drop of saturated NaNO₂ solution. The sample was equilibrated overnight. The sample was then placed in a Jasco J720 CD spectrometer (Japan Spectroscopic Co, Ltd, Tokyo) such that the tube-holder axis was parallel with the beam axis so that the beam was normal to the sample. The sample was rotated around the beam axis in increments of 45°. The CD spectra were collected for eight discrete angles and averaged.

X-ray diffraction

X-ray diffraction experiments were performed with Cu-K α radiation ($\lambda = 1.542 \text{ \AA}$) on an 18 kW rotating anode X-ray generator (Bruker AXS, Inc. (formerly Siemens, Inc.), Madison, WI) equipped with double-focusing mirrors (Charles Supper, Nattick, MA) operated at 38 kV and 30 mA using a 0.3 mm filament. The diffraction pattern was recorded on a Siemens X-1000 xenon-filled area detector with position decoding circuit and real-time data display. The collection of X-ray patterns and peak integration, and absorption correction was performed as described (Hristova & White, 1998).

Scaling of X-ray structure factors

The scaling of experimental X-ray structure factors to place them on the relative-absolute, or per-lipid, scale (Jacobs & White, 1989) has been described in detail (Wiener & White, 1991c; Hristova & White, 1998). Briefly, the experimental structure factors $f(h)$ from a given experiment depend upon the amount of sample in the beam, precise geometry of the sample-beam interaction, X-ray beam intensity, and other experimental conditions. The true (absolute) structure factors, $F(h)$, are determined solely by the scattering factor of the unit cell. The experimental structure factors are related to the true structure factors by $f(h) = KF(h)$, where K is the instrumental constant. Fourier reconstructions of bilayer scattering-length or electron density profiles yield only arbitrary fluctuations of scattering density along the bilayer normal if the average scattering-length density of the unit is not accounted for and if $f(h)$ rather than $F(h)$ is used. Determination of the instrumental constant allows one to relate the scattering profiles obtained in diffraction experiments to the actual contents and molecular packing of the bilayer unit cell. To do this, one must (1) determine the true mean value of the scattering profile using the composition of the unit cell and (2) calibrate the fluctuations around this mean value (Franks *et al.*, 1978; Wiener & White, 1991c; Hristova & White, 1998).

The scattering-length density $\rho^*(z)$ that describes the distribution of scattering matter along the bilayer normal z on a per lipid basis is given by (Jacobs & White, 1989):

$$\rho^*(z) = \rho(z)S = \rho_0^* + \frac{21}{dk} \sum_{h=1}^N f(h) \cos\left(\frac{2\pi hz}{d}\right) \quad (1)$$

In this equation $f(h)$ are the measured structure factors in arbitrary units, d is the Bragg spacing, N is the highest observable diffraction order, S is the area/lipid and $k = K/S$. With these definitions, the relative-absolute structure factors are given by $F^*(h) = f(h)/k$. The per-lipid scattering-length density $\rho^*(z)$ and its average ρ_0^* are obtained from the absolute (per unit area) scattering densities according to $\rho^*(z) = \rho(z)S$ and $\rho_0^* = \rho_0 S$. This per-lipid scaling allows data analysis without explicit knowledge of the lipid area.

The scaling of the structure factors is based on the incorporation of a strongly scattering "label" of known scattering length into the unit-cell without changing the unit cell structure (isomorphous replacement), and then determining the so-called difference structure (see Figure 2). In the present experiments, we labeled the double bond of the *sn*-2 chain of DOPC with two bromine atoms of scattering length $2b_{\text{Br}}$ to produce OBPC, which is isomorphous with DOPC (Wiener & White, 1991c; Hristova & White, 1998). The difference structure is the transbilayer distribution of the bromine atoms, described by a pair of Gaussian distributions of 1/e-half-width A_{Br} , located at $z = \pm Z_{\text{Br}}$:

$$\Delta\rho_{\text{Br}}^*(z) = \frac{2xb_{\text{Br}}}{A_{\text{Br}}\sqrt{\pi}} \left\{ \exp\left[-\left(\frac{z - Z_{\text{Br}}}{A_{\text{Br}}}\right)^2\right] + \exp\left[-\left(\frac{z + Z_{\text{Br}}}{A_{\text{Br}}}\right)^2\right] \right\} \quad (2a)$$

The structure factors $F_{\text{Br}}(h)$ of this distribution are given by (Wiener & White, 1991c):

$$F_{Br}(h) = 2xb_{Br} \exp[-(\pi A_{Br}h/d)^2] \cos(2\pi hZ_{Br}) \quad (2b)$$

Because the scattering length b_{Br} is known, fits of equation (2b) to the observed difference structure factors *via* non-linear least-squares minimization allows one to set the scale of the structure factors, as described below. To reduce the experimental uncertainties, average out random error, and assure that OBPC is isomorphous with DOPC, we examined a number of samples with different mole fractions x of OBPC.

Wiener & White (1991c) have described in detail a procedure for scaling multiple data sets that involves, in simple terms, re-scaling the structure factors so that the data sets are described by a set of internally consistent experimental constants. This is necessary because the scale factor K varies from one data collection run to the next due to differences in beam intensity, amount of sample, etc. Let the internally consistent per-lipid structure factors of pure OBPC bilayers be $F_A^*(h)$ and those of pure DOPC bilayers be $F_B^*(h)$. Because the two bilayers are isomorphous, the absolute structure factors for a bilayer with fraction x of OBPC will be:

$$F_x^*(h) = xF_A^* + (1-x)F_B^* \quad (3)$$

or:

$$\frac{f_x(h)}{k_x} = x \frac{f_A(h)}{k_A} + (1-x) \frac{f_B(h)}{k_B} \quad (4)$$

The scattering density profiles $\rho_A^*(z)$ and $\rho_B^*(z)$ can be calculated from equation (1) using the appropriate structure factors $f_A(z)$ and $f_B(z)$. These "basis" profiles are connected through the simple relationship:

$$\rho_A^*(z) = \rho_B^*(z) + \rho_{Br}^*(z) \quad (5)$$

where $\rho_{Br}^*(z)$ is the scattering density profile for the bromine atoms, given by equation (2). From equations (1), (2), (4), and (5), one obtains:

$$\frac{f_A(h)}{k_A} - \frac{f_B(h)}{k_B} = 2b_{Br} \exp[-(\pi A_{Br}h/d)^2] \cos(2\pi hZ_{Br}),$$

$$h = 1 \cdots h_{obs} \quad (6)$$

The system of h_{obs} equations allows one to determine k_A , k_B , A_{Br} , and Z_{Br} . The specific computational protocol has been described in detail (Hristova & White, 1998). The results of this protocol in the present case are shown in Figure 1. The data points are the observed per-lipid structure factors $F^*(h)$. The best statistical estimates of the structure factors $F^*(h)$ are found from the parameters of the best-fit straight line passing through the points. The error bars are obtained from the statistical uncertainties of the integrated intensities of the diffraction peaks taken as $(\text{peak area} + \text{background})^{1/2}$. Estimates of the experimental uncertainties in the Gaussian parameters was performed using the Monte Carlo procedure as described previously (Wiener & White, 1991c; Hristova & White, 1998; and see below).

Phasing of X-ray data

The specific labeling with bromine allows the determination of the phases of the X-ray structure factors (Franks *et al.*, 1978; Wiener & White, 1991c). All the terms in equation (2b), except for the cosine term, are positive-definite, and the sign of the cosine depends on h and Z_{Br} . Thus, the determined value of Z_{Br} defines the

phases (signs) of $F_x(h)$. The phases of the structure factors were already determined for pure DOPC at 66% RH (Wiener & White, 1991c). To scale the data, we assumed initially that the phases of the observed structure factors for DOPC do not change upon peptide insertion. This proved correct because for each value of h , the slope of $F_x(h)$ was in direction consistent with the determined Z_{Br} .

Perturbed-bilayer models

A simple re-scaling procedure was used to estimate the peptide-induced changes in the distributions of the lipid quasimolecular fragments comprising the bilayer structure (Jacobs & White, 1989). As shown by Wiener *et al.* (1991), the position of the Br-labeled distribution Z_{Br} coincides with the position Z_{CC} of double-bond distribution determined by means of neutron diffraction. The $1/e$ -halfwidth A_{Br} , however, is slightly larger than the true width of the double-bond distribution, A_{CC} , because the hard-sphere radius of the Br is convoluted with the thermal envelope of the double bond. We have shown that the double-bond distribution provides information about the physical state of the hydrocarbon core (Hristova & White, 1998). A comparison of the bromine distributions with and without peptide therefore reveals the changes in the HC core region that occur due to peptide insertion. Additional information about changes in bilayer structure is provided by the Bragg spacing, which reveals the over-all change in the bilayer thickness.

The structure of a fluid bilayer can be described by a collection of n transbilayer Gaussian distributions with parameters that account for the scattering density of the membrane unit cell (Wiener & White, 1991b, 1992b). If a peptide causes small perturbations in the bilayer structure as indicated by changes in Z_{Br} , A_{Br} , and d , then the changes in the n sets of Z_i and A_i are also expected to be small and to be linearly related to the changes in Z_{Br} , A_{Br} , and d (Jacobs & White, 1989). In the present case, $\Delta Z_{Br} = 0.65 \text{ \AA}$, $\Delta A_{Br} = 0$, and $\Delta(d/2) = -1.30 \text{ \AA}$. Because $\Delta A_{Br} = 0$, the two perturbed-bilayer models, model bilayer A and model bilayer B, were constructed in which the ΔA_i were taken as 0.

Model bilayer A assumes that the centers of the quasimolecular fragment distributions Z_i of the hydrocarbon core (methyl and methylene groups) shift in the same way as the bromine distribution:

$$Z_i^{\text{DOPC+18A}} = (Z_{Br}^{\text{DOPC+18A}}/Z_{Br}^{\text{DOPC}})Z_i^{\text{DOPC}} \quad (7)$$

while the centers of the interfacial quasimolecular fragments Z_j are assumed to shift towards the bilayer center relative to $Z_{Br}^{\text{DOPC+18A}}$ according to a scale factor:

$$\xi = [(d_{\text{DOPC+18A}} - 2Z_{Br}^{\text{DOPC+18A}})/(d_{\text{DOPC}} - 2Z_{Br}^{\text{DOPC}})] :$$

$$Z_j^{\text{DOPC+18A}} = \xi(Z_j^{\text{DOPC}} - Z_{Br}^{\text{DOPC}}) + Z_{Br}^{\text{DOPC+18A}} \quad (8)$$

Model bilayer B was constructed by assuming that all lipid quasimolecular fragments shift in proportion to the Bragg-spacing:

$$Z_k^{\text{DOPC+18A}} = (d_{\text{DOPC+18A}}/d_{\text{DOPC}})Z_k^{\text{DOPC}} \quad (9)$$

The water distributions of the models were treated similarly to the lipid quasimolecular fragments, except the

scattering length was taken as that of the number of water molecules per lipid molecule in the presence of the peptide, determined gravimetrically as described above.

Modeling the peptide structures in the bilayer

Structures of Ac-18A-NH₂ as a helix or an extended chain with different side-chain rotamer conformations were created using the software package Insight II (Biosym Technologies, San Diego, CA). In the construction of peptide structures, Insight II automatically chooses conformers that give side-chains maximally extended away from the peptide axis. Although such models led to successful fits with the experimental data, the *B*-factors required were found to be unreasonably small. To obtain more realistic side-chain conformers, we first manually selected side-chain conformers that gave compact structures, and then ran the Insight II minimization module to remove steric clashes. Molecular dynamics simulations were then run *in vacuo* for 5 ps at 300 K and 500 K in order to produce the models described in Results.

Representation of lipid and peptide in real and reciprocal space

Equation (2) in a generalized form provides the connection between the models and the observed structure factors. For a quasimolecular fragment of the bilayer or an atom of the peptide *i*, the transbilayer scattering-length density of *i* is given by:

$$\rho_i(z) = \frac{2b_i}{A_i\sqrt{\pi}} \left\{ \exp\left[-\left(\frac{z-Z_i}{A_i}\right)^2\right] + \exp\left[-\left(\frac{z+Z_i}{A_i}\right)^2\right] \right\} \quad (10a)$$

and its structure factors by:

$$F_i(h) = 2b_i \exp[-(\pi A_i h/d)^2] \cos(2\pi h Z_i) \quad (10b)$$

In order to simulate the scattering of the peptide in the bilayer, the scattering density of the atoms of the peptide models were projected on to the bilayer normal *z* in order to produce a one-dimensional peptide scattering density as described in Results. Each atom (*a*) was represented in this projection by a Gaussian scattering distribution whose thermal-motion envelope of 1/e-halfwidth *A_T* is determined by the choice of *B*-factor by the relation $B = 4\pi^2 A_T^2$. All atoms were assigned the same *B*-factor during the refinement procedure. The projected widths of the distribution of each atom are given by a Gaussian of 1/e-halfwidth *A_a* given by $A_a^2 = A_c^2 + A_T^2$ where *A_c* is the covalent radius of the atom (Pauling, 1960).

Structure refinement

The model transbilayer distribution of the peptide, represented by either the peptide structural models or simple Gaussian representing the total scattering length of the peptide scaled by the mol fraction of peptide in the bilayer, was superimposed on one of the bilayer models by addition of the structure factors. During the refinement, the model bilayer structure factors were held

constant, while the parameters describing the peptide models were varied. For the peptide models with given γ and η , the parameters varied were the *B*-factor and mean peptide position. For the Gaussian representation, the parameters used were the position *Z_p* and 1/e-halfwidth *A_p* of the peptide. The parameters were optimized using the standard Levenberg-Marquardt algorithm (Bevington, 1969; Press *et al.*, 1989) for the non-linear minimization of $R = \sum_h \left| \frac{\bar{F}^*(h)}{F_m(h)} - \frac{|F_m(h)|}{\sum_h |F^*(h)|} \right|$, where $\bar{F}^*(h)$ are the experimentally determined structure factors and *F_m*(*h*) are the structure factors of the DOPC/Ac-18A-NH₂ model. The quality of the experimental data was judged against the so-called self *R*-factor, defined as $R_{\text{self}} = \sum_h |\sigma_i(h)| / \sum_h |F^*(h)|$ (Wiener & White, 1991a), where the $\sigma_i(h)$ are the experimental uncertainties in the observed structure factors *F*^{*}(*h*). A fit was considered satisfactory if $R \leq R_{\text{self}}$.

The robustness of the fits and the uncertainties in *Z_p* and *A_p* in Step 3 were determined using the Monte Carlo sampling procedure by Wiener & White (1991b,c). This procedure is based upon the fact that each structure factor has an experimental uncertainty $\sigma(h)$ that can be used to define a normal distribution for each structure factor *F*^{*}(*h*). In simple terms, a Box-Muller algorithm (Ross, 1989) seeded with a random number is used to generate sets of "mock" structure factors from the observed *F*^{*}(*h*) and $\sigma(h)$. The mean and standard deviation of these mock sets will match those of the observed data. Although each set of mock data represents a statistically acceptable combination of structure factor amplitudes, each set will yield slightly different values for the parameters obtained in the refinement. The mean values and standard deviations of the collection of parameters describe the most likely values of the parameters and their uncertainties. If all of the sets of mock data lead to a convergence of the refinement, the fits can be considered robust.

Acknowledgments

This work was supported, in part, by grants GM-46823, PO1HL34343, PO134343, and AI-22931 from the National Institutes of Health. We thank Dr Alexey Ladoikhin for his comments on the manuscript.

References

- Anantharamaiah, G. M., Jones, J. L., Brouillette, C. G., Schmidt, C. F., Chung, B. H., Hughes, T. A., Bhowan, A. S. & Segrest, J. P. (1985). Studies of synthetic peptide analogs of the amphiphathic helix: Structure of complexes with dimyristoyl phosphatidylcholine. *J. Biol. Chem.* **260**, 10248-10255.
- Barlow, R. J. (1989). *Statistics. A Guide to the Use of Statistical Methods in the Physical Sciences*, pp. 1-204, John Wiley and Sons, New York.
- Bernèche, S., Nina, M. & Roux, B. (1998). Molecular dynamics simulation of melittin in a dimyristoyl-phosphatidylcholine bilayer membrane. *Biophys. J.* **75**, 1603-1618.
- Bevington, P. R. (1969). *Data Reduction and Error Analysis for the Physical Sciences*, pp. 1-336, McGraw-Hill Book Company, New York.
- Borhani, D. W., Rogers, D. P., Engler, J. A. & Brouillette, C. G. (1997). Crystal structure of truncated human

- apolipoprotein A-I suggests a lipid-bound conformation. *Proc. Natl Acad. Sci. USA*, **94**, 12291-12296.
- Bowie, J. U. (1997). Helix packing in membrane proteins. *J. Mol. Biol.* **272**, 780-789.
- Bradshaw, J. P., Dempsey, C. E. & Watts, A. (1994). A combined X-ray and neutron diffraction study of selectively deuterated melittin in phospholipid bilayers: effect of pH. *Mol. Membr. Biol.* **11**, 79-86.
- Brasseur, R. (1991). Differentiation of lipid-associating helices by use of three-dimensional molecular hydrophobicity potential calculations. *J. Biol. Chem.* **266**, 16120-16127.
- Brasseur, R., de Loof, H., Ruyschaert, J. M. & Rosseneu, M. (1988). Conformational analysis of lipid-associating proteins in a lipid environment. *Biochim. Biophys. Acta*, **943**, 95-102.
- Büldt, G., Gally, H. U., Seelig, A., Seelig, J. & Zaccai, G. (1978). Neutron diffraction studies on selectively deuterated phospholipid bilayers. *Nature*, **271**, 182-184.
- Clayton, A. H. A. & Sawyer, W. H. (1999). The structure and orientation of class-A amphipathic peptides on a phospholipid bilayer surface. *Eur. Biophys. J. Biophys. Letters*, **28**, 133-141.
- Cramer, W. A., Heymann, J. B., Schendel, S. L., Deriy, B. N., Cohen, F. S., Elkins, P. A. & Stauffacher, C. V. (1995). Structure-function of the channel-forming colicins. *Annu. Rev. Biophys. Biomol. Struct.* **24**, 611-641.
- Cross, T. A. & Opella, S. J. (1994). Solid-state NMR structural studies of peptides and proteins in membranes. *Curr. Opin. Struct. Biol.* **4**, 574-581.
- Deisenhofer, J., Epp, O., Miki, K., Huber, R. & Michel, H. (1985). Structure of the protein subunits in the photosynthetic reaction centre of *Rhodospseudomonas viridis* at 3 Å resolution. *Nature*, **318**, 618-624.
- Dempsey, C. E. (1990). The actions of melittin on membranes. *Biochim. Biophys. Acta*, **1031**, 143-161.
- Epand, R. M. (1993). *The Amphipathic Helix*, pp. 1-406, CRC Press, Boca Raton.
- Franks, N. P. & Levine, Y. K. (1981). Low-angle X-ray diffraction. In *Membrane Spectroscopy* (Grell, E., ed.), pp. 437-487, Springer-Verlag, Berlin.
- Franks, N. P., Arunachalam, T. & Caspi, E. (1978). A direct method for determination of membrane electron density profiles on an absolute scale. *Nature*, **276**, 530-532.
- Hristova, K. & White, S. H. (1998). Determination of the hydrocarbon core structure of fluid dioleoylphosphocholine (DOPC) bilayers by X-ray diffraction using specific bromination of the double-bonds: Effect of hydration. *Biophys. J.* **74**, 2419-2433.
- Huang, P. & Loew, G. H. (1995). Interaction of an amphiphilic peptide with a phospholipid bilayer surface by molecular dynamics simulation study. *J. Biomol. Struct. Dynam.* **12**, 937-956.
- Jacobs, R. E. & White, S. H. (1989). The nature of the hydrophobic binding of small peptides at the bilayer interface: Implications for the insertion of transbilayer helices. *Biochemistry*, **28**, 3421-3437.
- Jones, M. K., Anantharamaiah, G. M. & Segrest, J. P. (1992). Computer programs to identify and classify amphipathic α -helical domains. *J. Lipid Res.* **33**, 287-296.
- Kanellis, P., Romans, A. Y., Johnson, B. J., Kercret, H., Chioveti, R., Jr., Allen, T. M. & Segrest, J. P. (1980). Studies of synthetic peptide analogs of the amphipathic helix: Effect of charged amino acid residue topography on lipid affinity. *J. Biol. Chem.* **255**, 11464-11472.
- Katsaras, J. (1997). Highly aligned lipid membrane systems in the physiologically relevant "excess water" condition. *Biophys. J.* **73**, 2924-2929.
- Katsaras, J. (1998). Adsorbed to a rigid substrate, dimyristoylphosphatidylcholine multibilayers attain full hydration in all mesophases. *Biophys. J.* **75**, 2157-2162.
- King, G. I. & White, S. H. (1986). Determining bilayer hydrocarbon thickness from neutron diffraction measurements using strip-function models. *Biophys. J.* **49**, 1047-1054.
- Lund-Katz, S., Phillips, M. C., Mishra, V. K., Segrest, J. P. & Anantharamaiah, G. M. (1995). Microenvironments of basic amino acids in amphipathic α -helices bound to phospholipid: ^{13}C NMR studies using selectively labeled peptides. *Biochemistry*, **34**, 9219-9226.
- Makhataдзе, G. I., Medvedkin, V. N. & Privalov, P. L. (1990). Partial molar volumes of polypeptides and their constituent groups in aqueous solution over a broad temperature range. *Biopolymers*, **30**, 1001-1010.
- Maloy, W. L. & Kari, U. P. (1995). Structure-activity studies on magainins and other host defense peptides. *Biopolymers*, **37**, 105-122.
- Mishra, V. K., Palgunachari, M. N., Segrest, J. P. & Anantharamaiah, G. M. (1994). Interactions of synthetic peptide analogs of the class A amphipathic helix with lipids: evidence for the snorkel hypothesis. *J. Biol. Chem.* **269**, 7185-7191.
- Palgunachari, M. N., Mishra, V. K., Lund-Katz, S., Phillips, M. C., Adeyeye, S. O., Alluri, S., Anantharamaiah, G. M. & Segrest, J. P. (1996). Only the two end helices of eight tandem amphipathic helical domains of human apo A-I have significant lipid affinity: Implications for HDL assembly. *Arterioscler. Thromb. Vasc. Biol.* **16**, 328-338.
- Pauling, L. (1960). *The Nature of the Chemical Bond and the Structure of Molecules and Crystals: An Introduction to Modern Structural Chemistry*, 3rd edit., pp. 1-644, Cornell University Press, Ithaca.
- Petrache, H. I., Feller, S. E. & Nagle, J. F. (1997). Determination of component volumes of lipid bilayers from simulations. *Biophys. J.* **70**, 2237-2242.
- Press, W. H., Flannery, B. P., Teukolsky, S. A. & Vetterling, W. T. (1989). *Numerical Recipes. The Art of Scientific Computing*, pp. 1-702, Cambridge University Press, Cambridge.
- Ross, S. M. (1989). *Introduction to Probability Models*, 4th edit., pp. 1-544, Academic Press, San Diego.
- Segrest, J. P., Jackson, R. L., Morrisett, J. D. & Gotto, A. M., Jr (1974). A molecular theory for lipid-protein interactions in the plasma lipoproteins. *FEBS Letters*, **38**, 247-253.
- Segrest, J. P., Deloof, H., Dohlman, J. G., Brouillette, C. G. & Anantharamaiah, G. M. (1990). Amphipathic helix motif - classes and properties. *Proteins: Struct. Funct. Genet.* **8**, 103-117.
- Segrest, J. P., Jones, M. K., Deloof, H., Brouillette, C. G., Venkatachalapathi, Y. V. & Anantharamaiah, G. M. (1992). The amphipathic helix in the exchangeable apolipoproteins - a review of secondary structure and function. *J. Lipid Res.* **33**, 141-166.
- Segrest, J. P., Garber, D. W., Brouillette, C. G., Harvey, S. C. & Anantharamaiah, G. M. (1994). The amphipathic α helix: A multifunctional structural motif in

- plasma apolipoproteins. *Advan. Protein Chem.* **45**, 303-369.
- Segrest, J. P., Jackson, R. L., Morrisett, J. D. & Gotto, A. M., Jr (1998). A molecular theory of lipid-protein interactions in the plasma lipoproteins. *FEBS Letters*, **38**, 247-258.
- Spuhler, P., Anantharamaiah, G. M., Segrest, J. P. & Seelig, J. (1994). Binding of apolipoprotein A-I model peptides to lipid bilayers. Measurement of binding isotherms and peptide-lipid headgroup interactions. *J. Biol. Chem.* **269**, 23904-23910.
- Tossi, A., Tarantino, C. & Romeo, D. (1997). Design of synthetic antimicrobial peptides based on sequence analogy and amphipathicity. *Eur. J. Biochem.* **250**, 549-558.
- Tytler, E. M., Segrest, J. P., Epand, R. M., Nie, S. Q., Epand, R. F., Mishra, V. K., Venkatachalapathi, Y. V. & Anantharamaiah, G. M. (1993). Reciprocal effects of apolipoprotein and lytic peptide analogs on membranes: cross-sectional molecular shapes of amphipathic- α helices control membrane stability. *J. Biol. Chem.* **268**, 22112-22118.
- Tytler, E. M., Anantharamaiah, G. M., Walker, D. E., Mishra, V. K., Palgunachari, M. N. & Segrest, J. P. (1995). Molecular basis for prokaryotic specificity of magainin- induced lysis. *Biochemistry*, **34**, 4393-4401.
- Venkatachalapathi, Y. V., Phillips, M. C., Epand, R. M., Epand, R. F., Tytler, E. M., Segrest, J. P. & Anantharamaiah, G. M. (1993). Effect of end group blockage on the properties of a class A amphipathic helical peptide. *Proteins: Struct. Funct. Genet.* **15**, 349-359.
- Warren, B. E. (1969). *X-ray Diffraction*, pp. 1-381, Addison-Wesley, Reading, MA.
- White, S. H. & Wiener, M. C. (1995). Determination of the structure of fluid lipid bilayer membranes. In *Permeability and Stability of Lipid Bilayers* (Disalvo, E. A. & Simon, S. A., eds), pp. 1-19, CRC Press, Boca Raton.
- White, S. H. & Wiener, M. C. (1996). The liquid-crystallographic structure of fluid lipid bilayer membranes. In *Membrane Structure and Dynamics* (Merz, K. M. & Roux, B., eds), pp. 127-144, Birkhäuser, Boston.
- White, S. H. & Wimley, W. C. (1994). Peptides in lipid bilayers: structural and thermodynamic basis for partitioning and folding. *Curr. Opin. Struct. Biol.* **4**, 79-86.
- White, S. H. & Wimley, W. C. (1998). Hydrophobic interactions of peptides with membrane interfaces. *Biochim. Biophys. Acta*, **1376**, 339-352.
- White, S. H., Jacobs, R. E. & King, G. I. (1987). Partial specific volumes of lipid and water in mixtures of egg lecithin and water. *Biophys. J.* **52**, 663-665.
- Wiener, M. C. & White, S. H. (1991a). Fluid bilayer structure determination by the combined use of X-ray and neutron diffraction. I. Fluid bilayer models and the limits of resolution. *Biophys. J.* **59**, 162-173.
- Wiener, M. C. & White, S. H. (1991b). Fluid bilayer structure determination by the combined use of X-ray and neutron diffraction. II. "Composition-space" refinement method. *Biophys. J.* **59**, 174-185.
- Wiener, M. C. & White, S. H. (1991c). Transbilayer distribution of bromine in fluid bilayers containing a specifically brominated analog of dioleoylphosphatidylcholine. *Biochemistry*, **30**, 6997-7008.
- Wiener, M. C. & White, S. H. (1992a). Structure of a fluid dioleoylphosphatidylcholine bilayer determined by joint refinement of X-ray and neutron diffraction data. II. Distribution and packing of terminal methyl groups. *Biophys. J.* **61**, 428-433.
- Wiener, M. C. & White, S. H. (1992b). Structure of a fluid dioleoylphosphatidylcholine bilayer determined by joint refinement of x-ray and neutron diffraction data. III. Complete structure. *Biophys. J.* **61**, 434-447.
- Wiener, M. C., King, G. I. & White, S. H. (1991). Structure of a fluid dioleoylphosphatidylcholine bilayer determined by joint refinement of x-ray and neutron diffraction data. I. Scaling of neutron data and the distribution of double-bonds and water. *Biophys. J.* **60**, 568-576.
- Wimley, W. C. & White, S. H. (1996). Experimentally determined hydrophobicity scale for proteins at membrane interfaces. *Nature Struct. Biol.* **3**, 842-848.
- Wu, Y., Huang, H. W. & Olah, G. A. (1990). Method of oriented circular dichroism. *Biophys. J.* **57**, 797-806.
- Wu, Y., He, K., Ludtke, S. J. & Huang, H. W. (1995). X-ray diffraction study of lipid bilayer membranes interacting with amphiphilic helical peptides: diphytanoyl phosphatidylcholine with alamethicin at low concentrations. *Biophys. J.* **68**, 2361-2369.

Edited by D. C. Rees

(Received 21 December 1998; received in revised form 29 April 1999; accepted 30 April 1999)